Journal of Theoretical Biology 293 (2012) 219–235

Contents lists available at SciVerse ScienceDirect

Journal of Theoretical Biology

journal homepage: www.elsevier.com/locate/yjtbi

Mathematical model of GAL regulon dynamics in *Saccharomyces cerevisiae*

Raluca Apostu [a,*], Michael C. Mackey [b]

[a] Department of Physiology, McGill University, 3655 Promenade Sir William Osler, Montréal, Quebec, Canada H3G 1Y6
[b] Department of Physiology, Physics, Mathematics and Centre for Applied Mathematics in Bioscience and Medicine, McGill University, 3655 Promenade Sir William Osler, Montréal, Quebec, Canada H3G 1Y6

ARTICLE INFO

Article history:
Received 21 June 2011
Received in revised form
24 August 2011
Accepted 11 October 2011
Available online 19 October 2011

Keywords:
Mathematical modeling
Galactose induction
GAL regulon
Bistability
Saccharomyces cerevisiae

ABSTRACT

Genetic switches are prevalent in nature and provide cells with a strategy to adapt to changing environments. The GAL switch is an intriguing example which is not understood in all detail. The GAL switch allows organisms to metabolize galactose, and controls whether the machinery responsible for the galactose metabolism is turned on or off. Currently, it is not known exactly how the galactose signal is sensed by the transcriptional machinery. Here we utilize quantitative tools to understand the *S. cerevisiae* cell response to galactose challenge, and to analyze the plausible molecular mechanisms underlying its operation. We work at a population level to develop a dynamic model based on the interplay of the key regulatory proteins Gal4p, Gal80p, and Gal3p. To our knowledge, the model presented here is the first to reproduce qualitatively the bistable network behavior found experimentally. Given the current understanding of the GAL circuit induction (Wightman et al., 2008; Jiang et al., 2009), we propose that the most likely *in vivo* mechanism leading to the transcriptional activation of the GAL genes is the physical interaction between galactose-activated Gal3p and Gal80p, with the complex Gal3p–Gal80p remaining bound at the GAL promoters. Our mathematical model is in agreement with the flow cytometry profiles of wild type, *gal3Δ* and *gal80Δ* mutant strains from Acar et al. (2005), and involves a fraction of actively transcribing cells with the same qualitative features as in the data set collected by Acar et al. (2010). Furthermore, the computational modeling provides an explanation for the contradictory results obtained by independent laboratories when tackling experimentally the issue of binary versus graded response to galactose induction.

1. Introduction

Modeling the induction of GAL genes upon galactose challenge in *S. cerevisiae* cells is an intriguing problem. Although the key elements leading to induction have been known for decades (Lohr et al., 1995), an array of GAL system properties failed to be reproduced by the current dynamical models. For example, the binary response pattern after sugar induction (Acar et al., 2005), the galactose independent induction of the GAL machinery through GAL3 over expression (Bhat and Hopper, 1992), and the transcriptional memory (Kundu and Peterson, 2010) are some properties found experimentally that await understanding at a modeling level. Moreover, in the last couple of years we have witnessed the acquisition of novel evidence at the molecular level which sparked a spirited debate regarding the regulatory mechanisms leading to GAL genes activation (Wightman et al., 2008). The present study proposes a deterministic model of GAL regulon induction in a large population of *S. cerevisiae* cells, and uses this mathematical model to distinguish between competing theories, focusing on the bistable property of the network.

The organization of the paper is as follows. First, we describe briefly the physiology of the galactose utilization pathway and the induction of the GAL genes. Section 2.1 offers a concise overview of the key molecular elements in this process, and the contrasting theories supported by biochemical and genetic evidence. Next, we survey previous mathematical modeling studies of this system, pointing out briefly their contribution to a quantitative understanding of the system as well as their weaknesses (Section 2.2). Our modeling strategy is outlined in Section 2.3. The mathematical formulation of the two competing hypotheses at the GAL promoters, the protein–protein interactions, and the synthesis of novel proteins via transcription and translation following galactose induction is included in Section 3. The mathematical analysis of the two potential mechanisms leading to GAL gene induction after galactose challenge and the formulation of our deterministic model is finalized in Section 4. We compare our model behavior with experimental data in Sections 5.1 and 5.2, and we describe the model predictions in Section 5.3.

* Corresponding author. Tel.: +1 514 583 0180; fax: +1 514 398 7452.
E-mail addresses: raluca.apostu@mail.mcgill.ca (R. Apostu), michael.mackey@mcgill.ca (M.C. Mackey).

0022-5193/$ - see front matter © 2011 Elsevier Ltd. All rights reserved.
doi:10.1016/j.jtbi.2011.10.012

2. GAL regulon

Galactose is a monosaccharide which can be used as a carbon source by the unicellular fungus *Saccharomyces cerevisiae*. Its presence in the medium initiates the synthesis of the enzymes metabolizing galactose from the GAL gene cluster. Compared to glucose, which is the preferred carbon source, galactose is a poor sugar and its metabolism requires the synthesis of the Leloir enzymes (GAL1, GAL7, GAL10). The production of the Leloir enzymes is energetically expensive as they constitute approximately 5% of the total cellular protein content when yeast is grown on galactose as the sole carbon source (Bhat, 2008). If a mixture of these two sugars is available, a *S. cerevisiae* cell will preferentially use glucose over galactose. While galactose induces the GAL genes within minutes to very high levels ($\sim$1000 fold increase in GAL1 mRNA and about 3 fold increase in GAL3 expression), glucose triggers catabolite repression of the GAL regulon through multiple mechanisms (Ideker et al., 2001; Reece, 2000). In the presence of other carbon sources, such as non-repressing non-inducing sugars like raffinose or glycerol, the structural genes (GAL1, GAL7, GAL10) are switched off, while the regulatory genes (GAL80, GAL3, GAL4, GAL2) that control the expression of the structural genes are expressed at basal levels keeping the network poised for induction.

2.1. Induction of the GAL genes

The switch between inactive and active gene expression is modulated by the interplay of three key proteins: Gal3p, Gal80p, and Gal4p. Gal4p is a transcriptional activator that binds as a dimer to a 17bp upstream activator sequence at the GAL promoters (UASg). In the absence of galactose, the transcriptional repressor Gal80p physically associates with Gal4p to form a transcriptionally inert complex. Gal80p masks the activation domain of Gal4p and inhibits the recruitment of RNAP II at the promoters. When the galactose molecule enters the cell through the basal levels of the permease Gal2p, the transcriptional inducer Gal3p becomes activated, gains affinity for the repressor molecules, and forms a complex with the Gal80p monomers. Somehow this chemical reaction removes the repression at the GAL promoters, and Gal4p becomes active.

The fate of Gal80p molecules bound to the DNA–Gal4p complex in induced cells is the subject of a great deal of debate. Over the years, two distinct conceptual models of the GAL induction have been proposed. A series of experiments performed by independent laboratories led to the hypothesis that the transcription of the GAL genes is initiated via a tripartite complex of Gal4p, Gal80p, and Gal3p which is transcriptionally active. This hypothesis, known as the *non-dissociation model* (see Fig. 1, panel A), is derived mainly from the observation that Gal4p and Gal80p remain associated in galactose-induced cells (Parthun and Jaehning, 1992; Leuther and Johnston, 1992; Bhaumik et al., 2004), and from an *in vitro* electrophoresis mobility shift assay which reveals that the complex Gal4p–Gal3p–Gal80p remains associated with a DNA segment containing the UASg after galactose challenge (Platt and Reece, 1998). The results from Wightman et al. (2008) show that both Gal3p and Gal80p are nucleocytoplasmic proteins, and they interact throughout the cell in galactose-induced cells. In this scenario, it is believed that the interaction between Gal3p and Gal4p-bound Gal80p would cause Gal80p to shift its position from the site overlapping the activation domain of Gal4p to a second interaction site (Platt and Reece, 1998).

Starting in 2000, the work by Hopper and collaborators laid the foundation for a different model of GAL activation based on the nuclear depletion of the repressor and Gal80p dissociation from the DNA-bound Gal4p (Peng and Hopper, 2000, 2002). This view of the yeast galactose switch is known as the *nuclear depletion model*, and it laid the groundwork for the mathematical modeling work of Acar et al. (2005), Ramsey et al. (2006), and Bennett et al. (2008). The *nuclear depletion model* considered that Gal3p is an exclusively cytoplasmic protein which binds the repressor molecule upon its activation by galactose. The physical association of the two key molecules alters the balance of free nuclear-cytoplasmic Gal80p, leads to a nucleocytoplasmic shuttling of Gal80p, and renders Gal4p active. This model was based on several experimental observations. Immunofluorescence experiments and cell fractionation analysis revealed that Gal3p is present only in the cytoplasm, while Gal80p could be detected throughout the cell (Peng and Hopper, 2000). Moreover, the repressor molecule was shown to shuttle rapidly between nucleus and cytoplasm, and that the galactose induction was not impaired by anchoring Gal3p molecules to either inner plasma membrane and intracellular vesicle membranes, or outer mitochondrial membranes (Peng and Hopper, 2000, 2002).

To address some of these questions and the results challenging the *nuclear depletion model*, Hopper's group revised recently their experimental approach in Jiang et al. (2009). It was found that Gal3p was localized in both nucleus and cytosol before and after

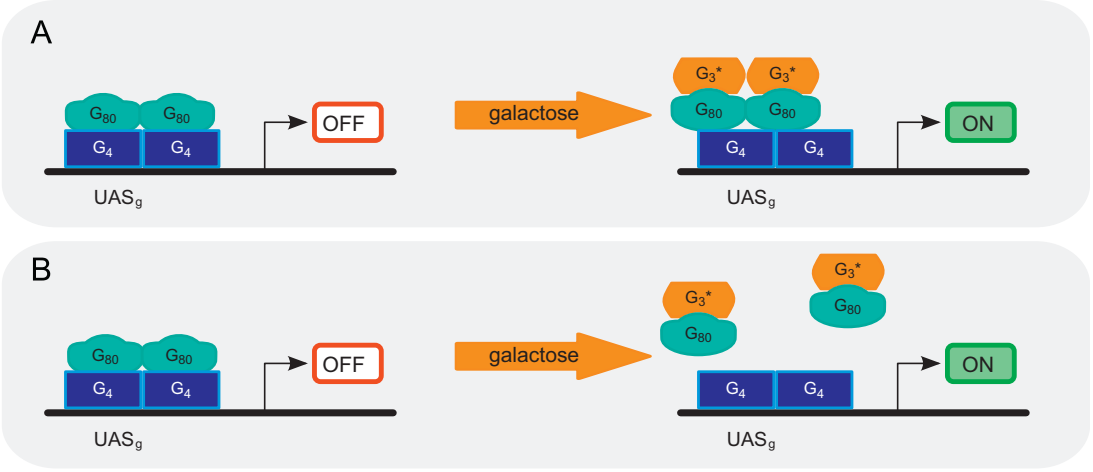

Fig. 1. Schematic representation of the two contrasting hypotheses for the molecular interactions at GAL promoters. The cartoon corresponds to a gene with a single UASg for Gal4p (G_4) homodimers. (a) *Non-dissociation model.* Gal3p* (G_3^*) interacts with the repressor and forms a tripartite complex with Gal80p (G_{80}) and DNA-bound Gal4p. (b) *Dissociation model.* Gal3p* interacts with Gal80p and dissociates from the DNA-bound Gal4p.

galactose challenge, and Gal80p showed a modest nuclear-to-cytoplasmic redistribution which occurred after the transcription was initiated. Consequently, the *nuclear depletion model* of the GAL switch lost its validity. The reporter array from Jiang et al. (2009) allowed the simultaneous monitoring of the temporal evolution of a reporter gene expression driven by GAL1 promoter, as well as the localization of both Gal4p and Gal80p proteins. Their evidence strengthened a *dissociation model* of Gal80p leaving the DNA–Gal4p complex upon galactose challenge (see Fig. 1, panel B), and suggested that this dissociation event is dependent on the Gal3p–Gal80p interaction. Previously, chromatin immunoprecipitation experiments from Peng and Hopper (2002) proposed the *dissociation model* as it was noticed that the occupancy of Gal80p on Gal4p at GAL promoters decreases as the concentration of galactose increases.

Currently, it is not known how the galactose signal is sensed by the transcriptional machinery, nor what the sequence of chemical reactions leading to the pathway activation is. Moreover, there are two contradictory hypotheses concerning the regulatory mechanism at GAL promoters in galactose-induced cells: the *dissociation* and *non-dissociation* models. Fig. 1 illustrates these. Nevertheless, there is agreement derived from the experimental evidence that the key reaction for the GAL induction is the interaction between Gal80p and Gal3p in a galactose and ATP-dependent manner. For example, when the association between the galactose-activated Gal3p and Gal80p is mutationally disabled, no expression of the reporter gene driven by the GAL1 promoter was observed even after 1 h of galactose challenge (Jiang et al., 2009).

2.2. Previous modeling work

Over the years, the induction of the GAL regulon by galactose has received attention from a several modeling groups. To our knowledge, the first attempt to model the GAL regulon was by Venkatesh et al. (1999). Other steady state models followed and started to build a quantitative knowledge of the GAL induction process. Among the various GAL properties addressed by the steady state models are the long term adaptation phenotype (Bhat and Venkatesh, 2005), the repression mechanisms involving Mig1p (Verma et al., 2005), the effect of the number of Gal4p binding sites at GAL promoters, and the relevance of the nucleo-cytoplasmic shuttling of the repressor (Verma et al., 2003).

Acar et al. (2005) began the series of the GAL dynamic models. They combined an experimental and quantitative approach to analyze the GAL network response to galactose induction, and used the yeast *S. cerevisiae* as a model system. The cells were pre-grown in either raffinose alone or a combination of raffinose and 2% galactose. Subsequently, the yeast were exposed to various concentrations of galactose, and the sugar concentration was maintained constant in the culture medium. After the steady state was reached, the network performance was quantified through the GFP expression driven by the GAL1 promoter and flow cytometry experiments. The flow cytometry profiles revealed two important characteristics of the regulatory mechanism. First, the GAL regulon has a transcriptional memory dependent on the growth history. Second, for some concentrations of galactose isogenic wild type cells can have two distinct gene expression states (ON and OFF), implying that the GAL network has a bistable response. The bistable property holds for *gal2Δ* and *gal80Δ* mutant cells. On the other hand, *gal3Δ* cells did not respond in a binary fashion. The bistable property of a wild type cell population upon galactose challenge was noted experimentally by Acar et al. (2010) as well as by other independent laboratories (Hawkins and Smolke, 2006; Song et al., 2010). The mathematical model of Acar et al. (2005) describes the changes in the total concentration of Gal3p in a strain disabled for GAL80 autoregulation under the assumption that all the protein-protein interactions between the key regulatory factors, as well as the activation of Gal3p, are rapid compared with the mRNA and protein production. The resulting bifurcation diagram shows the system behavior as a function of external galactose and Gal80p concentration.

The models from de Atauri et al. (2004), Orrell et al. (2006), and Ramsey et al. (2006) are produced by a common group of authors, have the same mathematical core, and are all based on a very similar mathematical formulation. Their perspective on GAL regulation design principles is discussed in de Atauri et al. (2004), while the sources and the mechanisms of controlling the intrinsic noise are the subject of Orrell et al. (2006). Ramsey et al. (2006) investigate the role of the network architecture, and focuses on the importance of GAL3 and GAL80 feedback loops. The experimental study done in this paper in conjunction with the modeling work involves a yeast strain pre-grown in 2% raffinose and then introduced to 0.1% galactose. The wild type cells have a graded response, while a cell population with a double GAL3–GAL80 knockout segregates into responding and non-responding cells within a few hours of induction. Although the model from Ramsey et al. (2006) successfully reproduces the fluorescence distribution of the reporter protein for both wild type and mutant disabled for GAL3 and GAL80 loops, their numerical experiments suggest that neither the wild type nor the mutant strain is capable of residing in multiple steady states. Bennett et al. (2008) extended the model from Ramsey et al. (2006) by adding a simple glucose regulatory module. The extended model was used in tandem with experimental results to gain some understanding of yeast metabolic gene regulation in response to sinusoidal perturbations in the environmental carbon sources.

Each of the mathematical models discussed in this section is a quantitative formulation based on the *nuclear depletion model*. Besides the experimental evidence discussed in the previous section which casts doubt on the veracity of the nuclear depletion model, Kumar et al. (2008) suspected that there might be a missing factor in such a hypothesis due to the rapid induction of the GAL genes. Additionally, Kulkarni et al. (2010) invoked mathematical arguments to conclude that a GAL circuit with an activation mechanism based on Gal3p sequestering the nucleo-cytoplasmic protein Gal80p in the nucleus is not able to display multiple steady states. Consequently, there appear to still be missing pieces in the GAL regulation puzzle, and much more work has to be done for a true understanding of the molecular events leading to the activation of the GAL regulon. The bistable response upon galactose induction remains unexplained at modeling level, along with the galactose independent induction of the GAL machinery through GAL3 overexpression (Bhat and Hopper, 1992), and the transcriptional memory (Kundu and Peterson, 2010). In the present study, we address the bistable property of the GAL regulon through a mathematical study.

2.3. Our modeling approach

The galactose utilization pathway consists of a biochemical route that metabolizes galactose, and a mechanism that controls whether the metabolic compartment is ON or OFF. The present study focuses on the genetic regulatory component which governs the activation of GAL genes when cells are switched from a non-inducing non-repressing carbon source (*e.g.*, raffinose) to galactose. Our model encompasses the dynamic change of the key components (Gal3p, Gal80p), and describes the main interactions leading to induction —namely, Gal3p activation by galactose, its interaction with Gal80p to relieve the transcription inhibition, and the transcription and translation of the key GAL elements. Since Gal4p plays no regulatory role in the induction process (Sellick and Reece, 2005), we exclude its dynamics from the modeling.

Our modeling strategy is to build up from the core of the circuit which is the induction mechanism at the GAL promoters. We compute the probability of gene expression in a population of yeast cells for both the *dissociation* and *non-dissociation hypotheses*, and select from the pool of potential scenarios the one explaining the bistability property. The idea of using quantitative tools to identify the most plausible mechanism from a pool of candidate models is the hallmark of mathematical modeling, and was initially used in this context by Verma et al. (2004). They formulated four models based on the subcellular localization of Gal3p* and its monomer versus dimer state. The most likely model was chosen by comparing the steady state model response and the experimentally collected fractional protein expression. Their study rules out the dimerization of Gal3p* as well as translocation of Gal3p* in the nucleus. However, this conclusion is in disagreement with experimental studies from two independent laboratories (Jiang et al., 2009; Wightman et al., 2008). Our modeling approach is different from Verma et al. (2004). We choose the correct mechanism at the promoter according to its ability to reproduce the bistable character of the network, and build a mathematical model based on the resulting analysis.

3. Model development

3.1. Two competing hypotheses

We start the quantitative study of the GAL regulon by considering the regulatory mechanism at the promoters. As mentioned previously, currently there are two contrasting theories regarding the initiation of induction (the *dissociation* and the *non-dissociation model*). Moreover, the GAL gene promoters have either one or more than two upstream binding sites for the transcriptional inducer Gal4p, and the number of binding sites is reflected at the transcription level. The regulatory genes (GAL3, GAL80) are driven by promoters with a single binding site, have a leaky expression in a non-inducing non-repressing medium, and the low levels of these proteins keep the system poised for induction (de Atauri et al., 2004). The structural genes have multiple binding sites (*e.g.*, GAL2 has two binding sites, GAL1 and GAL10 share four binding sites) and are tightly regulated. The tight regulation is most likely due either to the cooperative binding of the repressor molecules or to the reduced access of the transcriptional machinery to the [UASg:Gal4p:Gal80p] complex (Melcher and Xu, 2001; Bhat, 2008).

Our model reflects the effect of the number of binding sites through the *fractional transcription level* (known as well as the fraction of actively transcribing cells or the probability of the gene expression in a population), which we denote by F_n, where n represents the number of the binding sites for Gal4p dimers. The fractional transcription level is the only aspect of the model derivation which is model specific to either the *non-dissociation* or the *dissociation hypothesis*, and depends directly on the number of the binding sites. In the following two subsections we present the fractional transcription level for each case individually, and in Section 4.1 we investigate in which potential scenario the bistable response is possible. Since the expression of both GAL3 and GAL80 genes is governed by a promoter with a single UASg, we derive just the expression of F_1. The computations are fully shown here in the text for the *non-dissociation model*, while the *dissociation model* is treated similarly in Appendix B. Tables 1 and 2 summarize the possible sequences of chemical reactions and the corresponding expressions of F_1.

3.1.1. Non-dissociation hypothesis

First, we study the *non-dissociation hypothesis*. In response to an inducer, an individual cell may be either in an active or inactive state. Consequently, a cell population will segregate into responding and non-responding cells following galactose induction. Mathematically, the fraction of actively transcribing cells (or the probability of a gene being transcribed) is given by the ratio of the sum of the promoter configurations leading to transcription to the sum of all promoter configurations. Given the large number of Gal80p and Gal3p proteins in glucose [784 and 721 molecules, respectively] Ghaemmaghami et al., 2003 comparable to the total number of binding sites at the GAL promoters (only 22 molecules of Gal80p are necessary to repress transcription at the regulatory and structural GAL gene promoters (Bhat, 2008), we assume that the total concentration of both G_3 and G_{80} molecules is large.

The non-dissociation model assumes that the activated Gal3p forms a tripartite complex with Gal80p and DNA-bound Gal4p following galactose induction, *i.e.*

$$\begin{cases} 2G_{80} \rightleftharpoons^{\kappa_D} G_{80d}, \\ G_{80d} + D \rightleftharpoons^{\kappa_A} D_1, \\ 2G_3^* + D_1 \rightleftharpoons^{\kappa_B} D_2, \end{cases} \tag{1}$$

where

$$D \coloneqq [\text{UASg} : G_{4d}], \tag{2}$$

$$D_1 \coloneqq [\text{UASg} : G_{4d} : G_{80d}] = [D : G_{80d}], \tag{3}$$

$$D_2 \coloneqq [\text{UASg} : G_{4d} : G_{80d} : 2G_3^*] = [D_1 : 2G_3^*], \tag{4}$$

and $\kappa_D, \kappa_A, \kappa_B$ represent dissociation constants given by $\kappa_D = \kappa_D^- / \kappa_D^+$, $\kappa_A = \kappa_A^- / \kappa_A^+$, and $\kappa_B = \kappa_B^- / \kappa_B^+$ [see reactions (9), (10), (12), and

Table 1
Non-dissociation hypothesis. Fraction of ON cells (F_1) in a population where the expression is driven by a GAL promoter with a single upstream binding site (UASg) for Gal4p dimers. D and D_1 denote the complexes [UASg : G_{4d}] and [UASg : G_{4d} : G_{80d}], respectively. κ_A, κ_B, κ_B' and κ_D represent dissociation constants. In each case, the units of the dissociation constants are dictated by the underlying biochemistry.

Hypothesis	Set of chemical reactions	Probability of gene expression for one UASg for Gal4p	Bistable behavior
Non-dissociation model			
G_3^* monomers bind simultaneously	$2G_{80} \rightleftharpoons^{\kappa_D} G_{80d}$	$F_1^a = 1 - \frac{1}{1 + \frac{\kappa_A \kappa_D}{G_{80}^2} + \frac{(G_3^*)^2}{\kappa_B}}$	Yes
to [UASg : G_{4d} : G_{80d}].	$D + G_{80d} \rightleftharpoons^{\kappa_A} D_1$ $2G_3^* + D_1 \rightleftharpoons^{\kappa_B} [D_1 : 2G_3^*]$		
G_3^* monomers bind sequentially	$2G_{80} \rightleftharpoons^{\kappa_D} G_{80d}$	$F_1^b = 1 - \frac{1}{1 + \frac{\kappa_A \kappa_D}{G_{80}^2} + \frac{G_3^*}{\kappa_B} + \frac{(G_3^*)^2}{\kappa_B \kappa_B'}}$	Yes
to [UASg : G_{4d} : G_{80d}].	$D + G_{80d} \rightleftharpoons^{\kappa_A} D_1$ $G_3^* + D_1 \rightleftharpoons^{\kappa_B} [D_1 : G_3^*]$ $G_3^* + [D_1 : G_3^*] \rightleftharpoons^{\kappa_B'} [D_1 : 2G_3^*]$		

Table 2
Dissociation hypothesis. Fraction of ON cells (F_1) in a population where the expression is driven by a GAL promoter with a single upstream binding site (UASg) for Gal4p dimers. D denotes the complex [UASg : G_{4d}]. κ_A, κ_B, κ'_B, κ_C, and κ_D represent dissociation constants. In each case, the units of the dissociation constants are again dictated by the underlying biochemistry.

Hypothesis	Set of chemical reactions	Probability of gene expression for one UASg for Gal4p	Bistable behavior
Dissociation model			
G_3^* monomers bind simultaneously	$2G_{80} \rightleftharpoons^{\kappa_D} G_{80d}$	$F_1^c = \frac{1}{1+\kappa_B\frac{[G_3^*:G_{80}]^2}{(G_3^*)^2}} = \frac{1}{1+\frac{G_{80}^2}{\kappa_A\kappa_D}}$	No
to [UASg : G_{4d} : G_{80d}].	$D+G_{80d} \rightleftharpoons^{\kappa_A} [D : G_{80d}]$ $2G_3^*+[D : G_{80d}] \rightleftharpoons^{\kappa_B} D+2[G_3^* : G_{80}]$		
G_3^* monomers bind sequentially	$2G_{80} \rightleftharpoons^{\kappa_D} G_{80d}$	$F_1^d = 1-\frac{1}{1+\frac{G_3^*}{\kappa_B[G_3^*:G_{80}]}+\frac{\kappa_A\kappa_D}{G_{80}^2}}$	No
to [UASg : G_{4d} : G_{80d}].	$D+G_{80d} \rightleftharpoons^{\kappa_A} [D : G_{80d}]$ $G_3^*+[D : G_{80d}] \rightleftharpoons^{\kappa_B} [D : G_{80}]+[G_3^* : G_{80}]$	$= 1-\frac{1}{1+\sqrt{\frac{\kappa_A\kappa_D\kappa'_B}{\kappa_B}\frac{1}{G_{80}}}+\frac{\kappa_A\kappa_D}{G_{80}^2}}$	
	$G_3^*+[D : G_{80}] \rightleftharpoons^{\kappa'_B} D+[G_3^* : G_{80}]$		

Table 1]. At equilibrium, from (1) we have:

$$\kappa_D = \frac{G_{80}^2}{G_{80d}} \Rightarrow G_{80d} = \frac{G_{80}^2}{\kappa_D},$$

$$\kappa_A = \frac{D\cdot G_{80d}}{D_1} \Rightarrow D = \frac{\kappa_A\kappa_D}{G_{80}^2}D_1,$$

$$\kappa_B = \frac{(G_3^*)^2 D_1}{D_2} \Rightarrow D_2 = \frac{(G_3^*)^2}{\kappa_B}D_1.$$

The total concentration of the promoter is $D_T = D+D_1+D_2$, and the only promoter configurations leading to transcription are D and D_2. Therefore

$$F_1^a(G_3^*,G_{80}) = \frac{D+D_2}{D_T} = \frac{\frac{\kappa_A\kappa_D}{G_{80}^2}D_1+\frac{(G_3^*)^2}{\kappa_B}D_1}{\frac{\kappa_A\kappa_D}{G_{80}^2}D_1+D_1+\frac{(G_3^*)^2}{\kappa_B}D_1} = \frac{\frac{\kappa_A\kappa_D}{G_{80}^2}+\frac{(G_3^*)^2}{\kappa_B}}{1+\frac{\kappa_A\kappa_D}{G_{80}^2}+\frac{(G_3^*)^2}{\kappa_B}} = 1-\frac{1}{1+\frac{\kappa_A\kappa_D}{G_{80}^2}+\frac{(G_3^*)^2}{\kappa_B}}. \quad (5)$$

Similarly, if the G_3^* monomers bind sequentially to D_1 (see Table 1), the fraction of the cells in the induced state is

$$F_1^b(G_3^*,G_{80}) = 1-\frac{1}{1+\frac{\kappa_A\kappa_D}{G_{80}^2}+\frac{G_3^*}{\kappa_B}+\frac{(G_3^*)^2}{\kappa_B\kappa'_B}}. \quad (6)$$

3.1.2. Dissociation hypothesis

Analysis of the *dissociation model* proceeds in a similar fashion (c.f. Appendix B), again with the assumption that the total concentration of both G_3 and G_{80} molecules is large. The simultaneous binding of G_3^* molecules to [UASg : G_{4d} : G_{80d}] leads to Eq. (7), and the sequentially binding of G_3^* monomers to the same complex to an F_1 given by Eq. (8)

$$F_1^c(G_3^*,G_{80}) = \frac{1}{1+\kappa_B\frac{[G_3^*:G_{80}]^2}{(G_3^*)^2}}, \quad (7)$$

$$F_1^d(G_3^*,G_{80}) = 1-\frac{1}{1+\frac{G_3^*}{\kappa_B[G_3^*:G_{80}]}+\frac{\kappa_A\kappa_D}{G_{80}^2}}. \quad (8)$$

See Table 2 for the sequence of the chemical reactions and the meaning of the equilibrium dissociation constants κ_A, κ_B, κ'_B, and κ_D.

3.2. Deterministic induction of the GAL genes in a population of cells

Modeling assumptions: To avoid producing a large and unwieldy model, and to circumvent the current debate on the cellular localization of the key proteins before and after galactose challenge, we choose to not distinguish between nuclear and cytoplasmic components of the GAL molecules. Since gel filtration experiments show that Gal3p is monomeric in solution even at high concentrations (Timson et al., 2002), we assume that either Gal3p or Gal3p* dimerizes. Given that Gal80p dimerizes with high affinity (Melcher and Xu, 2001), we expect free Gal80p exists in a dimer form. Gal3p binds Gal80p in a 1:1 monomer-to-monomer ratio (Timson et al., 2002). Consequently, we consider the complex formed by Gal3p* and Gal80p to have 1:1 stoichiometry.

Set of chemical reactions: As an example, we consider the case of the *non-dissociation hypothesis*. Under both non-inducing non-repressing sugars and galactose as a primary carbon source, the transcriptional activator Gal4p binds as a dimer to a 17bp upstream activator sequence at GAL promoters. The repressor Gal80p physically associates with Gal4p to form a transcriptionally inert complex, masks the activation domain of Gal4p, and inhibits the recruitment of RNA polymerase II at the promoters. The entry of galactose into the cell is mediated by the galactose permease Gal2p. The internal galactose activates Gal3p, activated Gal3p physically interacts with both free and Gal4p-bound Gal80p, and relieves Gal80p repression (Lohr et al., 1995; Reece, 2000). This sequence of events is summarized by the following set of chemical reactions:

$$2G_{80} \rightleftharpoons^{\kappa_D^+}_{\kappa_D^-} G_{80d}, \quad (9)$$

$$G_{80d}+D \rightleftharpoons^{\kappa_A^+}_{\kappa_A^-} D_1, \quad (10)$$

$$G_3 \rightleftharpoons^{\nu(G_{\text{int}})}_{\kappa_r} G_3^*, \quad (11)$$

$$2G_3^*+D_1 \rightleftharpoons^{\kappa_B^+}_{\kappa_B^-} D_2, \quad (12)$$

$$2G_3^*+G_{80d} \rightleftharpoons^{\kappa_C^+}_{\kappa_C^-} 2[G_3^* : G_{80}], \quad (13)$$

where

$$D := [UAS_g : G_{4d}], \quad (14)$$

$$D_1 := [UAS_g : G_{4d} : G_{80d}] = [D : G_{80d}]. \quad (15)$$

$$D_2 := [UAS_g : G_{4d} : G_{80d} : 2G_3^*] = [D_1 : 2G_3^*]. \tag{16}$$

Quasi-steady-state assumption: The Gal80 dimerization, the DNA–protein binding and unbinding as well as the protein-protein interactions occur on a faster time scale than transcription, translation, and the degradation processes (Acar et al., 2005; Melcher and Xu, 2001). Therefore, the reactions (9), (10) and (12), (13) are considered at equilibrium, and the steady state concentrations of G_{80d}, D_1, D_2, and $[G_3^* : G_{80}]$ are given in terms of the dissociation equilibrium constants

$$\begin{cases} G_{80d} = \dfrac{G_{80}^2}{\kappa_D}, \\ D_1 = \dfrac{G_{80d} D}{\kappa_A} = \dfrac{G_{80}^2 D}{\kappa_A \kappa_D}, \\ D_2 = \dfrac{(G_3^*)^2 D_1}{\kappa_B} = \dfrac{G_{80}^2 (G_3^*)^2 D}{\kappa_A \kappa_B \kappa_D}, \\ [G_3^* : G_{80}] = \sqrt{\dfrac{(G_3^*)^2 G_{80d}}{\kappa_C}} = \dfrac{G_3^* G_{80}}{\sqrt{\kappa_C \kappa_D}}. \end{cases} \tag{17}$$

Note that $\kappa_D = \kappa_D^-/\kappa_D^+$, $\kappa_A = \kappa_A^-/\kappa_A^+$, and $\kappa_B = \kappa_B^-/\kappa_B^+$.

Modeling Gal3p activation: A key element in modeling and finding a possible mechanism that leads to bistability is the formulation of Gal3p activation by internal galactose

$$G_3 \underset{\kappa_r}{\overset{\nu(G_{\text{int}})}{\rightleftharpoons}} G_3^*. \tag{18}$$

Currently, it is not known how this process occurs. It is believed that it involves a conformational change (Wightman et al., 2008; Bhat and Murthy, 2001) but we are not aware of experimental evidence to support this. Hence we assume that the activation of Gal3p* by galactose follows a Michaelis-Menten type relationship:

$$\nu(G_{\text{int}}) = G_3 \kappa_{\text{cat}} \frac{G_{\text{int}}}{K_S + G_{\text{int}}}. \tag{19}$$

K_S and κ_{cat} are the half saturation constant and the catalytic constant, respectively.

Modeling the transcription of GALi genes for $i \in \{3, 80\}$. The rate of change of the GALi mRNA (M_i) transcribed from a promoter with n binding sites for Gal4p is governed by the difference between the production and the loss. The production term is defined as the product of the probability of a gene being transcribed (F_n) and the transcription rate ($\kappa_{\text{transcr,i}}$). This term reflects that the transcription is determined by the cellular concentration of the repressor (G_{80}), the inducing sugar (G_{int}), and the molecule triggering the transcription initiation (G_3) through the concentration of G_3^*. The loss is due to both intrinsic degradation (at a rate γ_{M_i}) and dilution (at a rate μ_M). Thus we write

$$\frac{dM_i}{dt} = \kappa_{\text{transcr,i}} F_{\text{n}}(G_3^*, G_{80}) - (\gamma_{M_i} + \mu_M) M_i. \tag{20}$$

Modeling the translation of GALi genes for $i \in \{3, 80\}$. Similarly, the rate of change of the GALi protein (G_i) is given by the difference between the quantity being translated from the mRNA at rate $\kappa_{\text{transl,i}}$, and the loss due both to intrinsic degradation (γ_{G_i}) and dilution (μ_G). Or

$$\frac{dG_i}{dt} = \kappa_{\text{transl,i}} M_i - (\gamma_{G_i} + \mu_G) G_i. \tag{21}$$

3.2.1. GAL dynamics in continuous culture

With the foregoing discussion in mind, we simulate the dynamics of the GAL gene synthesis in a cell population which is fed at a continuous constant rate of galactose (*i.e.*, $G_{\text{int}} = \text{constant}$) with a model consisting of the following system of five ordinary differential equations:

$$\begin{cases} \dfrac{dM_3}{dt} = F_1(G_3^*, G_{80}) \kappa_{\text{transc,3}} - (\gamma_{M_3} + \mu_M) M_3, \\ \dfrac{dG_3}{dt} = \kappa_{\text{transl,3}} M_3 - (\gamma_{G_3} + \mu_G) G_3 - G_3 \kappa_{\text{cat}} \dfrac{G_{\text{int}}}{K_S + G_{\text{int}}}, \\ \dfrac{dG_3^*}{dt} = G_3 \kappa_{\text{cat}} \dfrac{G_{\text{int}}}{K_S + G_{\text{int}}} - (\gamma_{G_3} + \mu_G) G_3^*, \\ \dfrac{dM_{80}}{dt} = F_1(G_3^*, G_{80}) \kappa_{\text{transc,80}} - (\gamma_{M_{80}} + \mu_M) M_{80}, \\ \dfrac{dG_{80}}{dt} = \kappa_{\text{transl,80}} M_{80} - (\gamma_{G_{80}} + \mu_G) G_{80} \end{cases} \tag{22}$$

and the set of the algebraic relations defining G_{80d}, D_1, D_2 and $[G_3^* : G_{80}]$. These algebraic relations result from the quasi-steady-state assumption and have been calculated for the case of the *non-dissociation model* (see Section 3.2 and (17)).

In the model development we assumed that the transcription of GAL3 and GAL80 follows from (20), and the translation of these genes is described according to (21). The activation of Gal3p by galactose is modeled as in (19). Since the GAL genes have a rapid induction, and the binding of galactose to Gal3p triggers the activation pathway, we assume that the rate κ_r of Gal3p* dissociating into Gal3p and galactose is negligible. The fraction of actively transcribing cells, F_1, is given by any of the functions F_1^a–F_1^d given by (6)–(8). In Section 4.1 we will study these, and determine which situation can explain the bistable response of the circuit.

4. Qualitative study of competing hypotheses at GAL promoters

Given the uncertainty of galactose signal propagation through the cell, and the contradictory regulatory mechanisms at GAL promoters, we use mathematical tools to distinguish between potential situations. Our strategy is to select from the pool of plausible mechanisms the ones explaining the network property of displaying multiple steady states.

4.1. Dissociation versus non-dissociation hypothesis: number of steady states

We analyze the mathematical model for a given G_{int}. This situation is equivalent to an experimental set up where the cells are fed at a continuous constant rate of galactose. At steady state, all temporal derivatives are set to zero so the ordinary differential equation model (22) reduces to

$$\begin{cases} M_3 = \dfrac{\kappa_{\text{transcr,3}}}{\gamma_{M_3} + \mu_M} F_1(G_3^*, G_{80}), \\ G_3^* = \overline{K} \dfrac{G_3 G_{\text{int}}}{G_{\text{int}} + K_S}, \\ G_3 = \dfrac{\kappa_{\text{transl,3}}}{\gamma_{G_3} + \mu_G + \kappa_{\text{cat}} \frac{G_{\text{int}}}{K_S + G_{\text{int}}}} M_3, \\ M_{80} = \dfrac{\kappa_{\text{transcr,80}}}{\gamma_{M_{80}} + \mu_M} F_1(G_3^*, G_{80}), \\ G_{80} = \dfrac{\kappa_{\text{transl,80}}}{\gamma_{G_{80}} + \mu_G} M_{80}, \end{cases} \tag{23}$$

where $F_1 \in \{F_1^a, F_1^b, F_1^c, F_1^d\}$ and $\overline{K} := \kappa_{\text{cat}}/(\gamma_{G_3} + \mu_G)$. Consequently, the protein steady state levels of G_3 and G_{80} satisfy the algebraic system

$$\begin{cases} AG_3 = F_1(G_3^*, G_{80}), \\ BG_{80} = F_1(G_3^*, G_{80}). \end{cases} \tag{24}$$

Since G_{int} is fixed, A and B defined by

$$A := \frac{(\gamma_{M_3}+\mu_M)\left(\gamma_{G_3}+\mu_G+\kappa_{\text{cat}}\frac{G_{\text{int}}}{K_S+G_{\text{int}}}\right)}{\kappa_{\text{transl},3}\kappa_{\text{transc},3}}, \tag{25}$$

$$B := \frac{(\gamma_{M_{80}}+\mu_M)(\gamma_{G_{80}}+\mu_G)}{\kappa_{\text{transl},80}\kappa_{\text{transc},80}}, \tag{26}$$

are constant. Note that the stationary values of the Gal3p and Gal80p protein are proportional to each other ($AG_3 = BG_{80} \Leftrightarrow G_{80} = AG_3/B$). Therefore G_{80} values are uniquely defined by G_3, and vice versa. Consequently, studying the number of the steady states of (24) is equivalent to finding the stationary values of either

$$AG_3 = F_1(G_3^*, G_{80}) \quad \text{with } G_{80} = \frac{A}{B}G_3 \tag{27}$$

or

$$BG_{80} = F_1(G_3^*, G_{80}) \quad \text{with } G_3 = \frac{B}{A}G_{80}. \tag{28}$$

In the remainder of this section, we investigate the steady states of (27) for each fractional transcription level function F_1^a, F_1^b, F_1^c, and F_1^d as calculated in Sections 3.1.1 and 3.1.2, and summarized in Tables 1 and 2. The mathematical expressions for $F_1^a - F_1^d$ are:

$$F_1^a(G_3^*, G_{80}) = 1 - \frac{1}{1+\frac{\kappa_A\kappa_D}{G_{80}^2}+\frac{(G_3^*)^2}{\kappa_B}},$$

$$F_1^b(G_3^*, G_{80}) = 1 - \frac{1}{1+\frac{\kappa_A\kappa_D}{G_{80}^2}+\frac{G_3^*}{\kappa_B}+\frac{(G_3^*)^2}{\kappa_B\kappa_B'}},$$

$$F_1^c(G_{80}) = \frac{1}{1+\frac{G_{80}^2}{\kappa_A\kappa_D}},$$

$$F_1^d(G_{80}) = 1 - \frac{1}{1+\sqrt{\frac{\kappa_A\kappa_D\kappa_B'}{\kappa_B}}\frac{1}{G_{80}}+\frac{\kappa_A\kappa_D}{G_{80}^2}}.$$

Since the steady states levels of G_3^* are dictated by the concentrations of G_3 and G_{int} (see (23)) it follows that

$$F_1^a(G_3^*, G_{80}) = F_1^a(G_3, G_{80}, G_{\text{int}}) = 1 - \frac{1}{1+\frac{\kappa_A\kappa_D}{G_{80}^2}+\frac{(G_3)^2}{\kappa_B}\left(\frac{\overline{K}G_{\text{int}}}{G_{\text{int}}+K_S}\right)^2}, \tag{29}$$

$$F_1^b(G_3^*, G_{80}) = F_1^b(G_3, G_{80}, G_{\text{int}}) = 1 - \frac{1}{1+\frac{\kappa_A\kappa_D}{G_{80}^2}+\frac{G_3}{\kappa_B}\frac{\overline{K}G_{\text{int}}}{G_{\text{int}}+K_S}+\frac{(G_3)^2}{\kappa_B\kappa_B'}\left(\frac{\overline{K}G_{\text{int}}}{G_{\text{int}}+K_S}\right)^2}. \tag{30}$$

Non-dissociation model: $\mathbf{F_1^a}$ *and* $\mathbf{F_1^b}$. At a steady state $G_{80} = AG_3/B$. We substituted G_{80} as a function of G_3 in F_1^a and F_1^b, and we plotted the resulting expressions as a function of G_3. Fig. 2, left panel, is a graphical display of the number of solutions of the system (27). F_1^a and F_1^b can have either one ($G_{3,1}^S$ or $G_{3,3}^S$), two ($G_{3,1}^S$, $G_{3,2}^S = G_{3,3}^S$ or $G_{3,1}^S = G_{3,2}^S$, $G_{3,3}^S$) or three ($G_{3,1}^S$, $G_{3,2}^S$, $G_{3,3}^S$) intersection points with the line AG_3 of slope A passing through the origin. Each of these intersection points corresponds to a steady state solution of the system (23). The ordering of the steady states is $0 < G_{3,1}^S \le G_{3,2}^S \le G_{3,3}^S$. The smallest of these ($G_{3,1}^S$) corresponds to an uninduced state while the largest ($G_{3,3}^S$) reflects an induced state. As shown in the next section, if $G_{3,2}^S$ exists, it is always unstable and would not be observable experimentally. For each solution G_3^S there is a uniquely defined G_{80}^S.

Dissociation model: $\mathbf{F_1^c}$ *and* $\mathbf{F_1^d}$. F_1^c and F_1^d are monotone decreasing functions of G_{80}. Their intersection with the line BG_{80} of slope B passing through the origin consists of an unique point G_{80}^S. This means that (28) has a unique steady state G_{80}^S solution to which corresponds an uniquely defined G_3^S, and thus cannot in principle ever lead to bistable behavior as observed in the GAL regulon.

For the *non-dissociation model*, the function F_1^a has a minimum at a value of G_3 that we denote by $\tilde{G}_3$, and at that point $F_1^{a\prime}(\tilde{G}_3) = 0$. Note that with the ordering of the steady states of the previous section, there are two cases to distinguish:

- Case I. $0 < \tilde{G}_3 \le G_{3,1}^S \le G_{3,2}^S \le G_{3,3}^S$. This case is illustrated in Fig. 2, left panel, and from our parameter estimations corresponds to the case that would be expected in the experimental

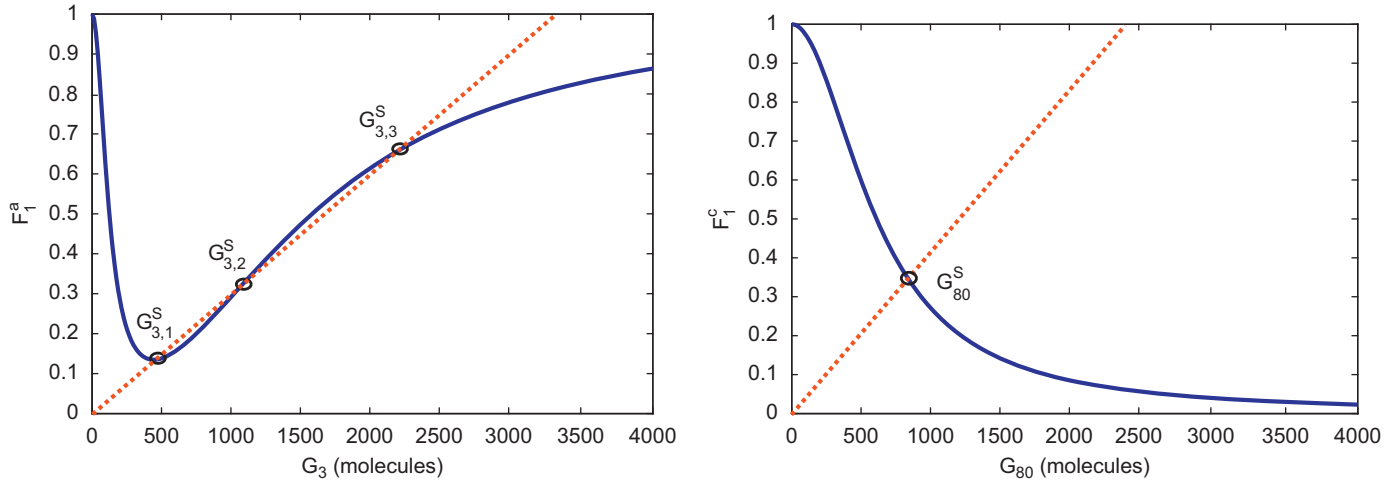

Fig. 2. Graphical illustration of the number of stationary solutions of the systems (27) and (28) for a given G_{int}. F_1^a and F_1^b have the same qualitative behavior with respect to G_3. The same holds for F_1^c and F_1^d with respect to G_{80}. Hence we include only the plot of F_1^a and F_1^c. Left panel: *Non-dissociation model*. F_1^a intersects the line of slope A passing through the origin in one, two, or three points depending on the slope A. This situation may lead to bistability (see the text). Right panel: *Dissociation model*. F_1^c is a monotone decreasing function of the repressor concentration. It intersects the line of slope B passing through the origin at a single point. The parameters used to generate F_1^a and F_1^c are $G_{\text{int}} = 1$ mM, $\kappa_{\text{cat}} = 300\ \text{min}^{-1}$, $K_S = 4000$ mM, $\kappa_{\text{transl},3} = 12.33\ \text{min}^{-1}$, $\kappa_{\text{transl},80} = 10.08\ \text{min}^{-1}$, $\kappa_A = 7 \times 10^{-4}$ mM. All the other parameters are listed in Table C2.

situations we are considering in this paper. In Appendix E, we have studied the stability of these steady states, showing that if $G^S_{3,2}$ exists then it is always unstable. This result shows that for the *non-dissociation model* there will either be one of two globally stable steady states ($G^S_{3,1}$ or $G^S_{3,3}$), or two co-existing locally stable steady states ($G^S_{3,1}$ and $G^S_{3,3}$).

- Case II. $0 < G^S_{3,1} \le \tilde{G}_3 \le G^S_{3,2} \le G^S_{3,3}$. This case is shown in Fig. E2 and has been considered in the Appendix E, but will not be dealt with further here as the parameter estimation appears to exclude it.

These results imply that the *non-dissociation model* is the only sufficient *in vivo* hypothesis of the two that we have examined, and that either the simultaneous or the sequential binding of the G_3^* monomers to the Gal4p-bound Gal80p can explain the bistability in the GAL response to galactose induction. Moreover, the bistable character of the *non-dissociation model* is robust to variations in the number of Gal4p binding sites (see Appendix A).

Consequently, in the remainder of this paper we focus our attention on the model of the *non-dissociation hypothesis*, and we choose F_1^q (Eq. (29)) as the fraction of the actively transcribing cells in a population due to the reduced number of parameters. For simplicity, we denote it by F_1

$$F_1(G_3^*,G_{80}) = 1 - \frac{1}{1+\frac{\kappa_A\kappa_D}{G_{80}^2}+\frac{(G_3^*)^2}{\kappa_B}} \tag{31}$$

In summary, to simulate the induction of the GAL regulon in a medium with a continuous source of galactose, we propose a model built on the *non-dissociation hypothesis*, and which comprises a system of five ordinary differential equations (Eqs. (22)) and four algebraic relations (Eqs. (17)). The fraction of actively expressing cells is defined by (31). For clarity, we reproduce the whole *non-dissociation model* below

$$\begin{cases} \dfrac{dM_3}{dt} = F_1(G_3^*,G_{80})\kappa_{\text{transc},3} - (\gamma_{M_3}+\mu_M)M_3, \\ \dfrac{dG_3}{dt} = \kappa_{\text{transl},3}M_3 - (\gamma_{G_3}+\mu_G)G_3 - G_3\kappa_{\text{cat}}\dfrac{G_{\text{int}}}{K_S+G_{\text{int}}}, \\ \dfrac{dG_3^*}{dt} = G_3\kappa_{\text{cat}}\dfrac{G_{\text{int}}}{K_S+G_{\text{int}}} - (\gamma_{G_3}+\mu_G)G_3^*, \\ \dfrac{dM_{80}}{dt} = F_1(G_3^*,G_{80})\kappa_{\text{transc},80} - (\gamma_{M_{80}}+\mu_M)M_{80}, \\ \dfrac{dG_{80}}{dt} = \kappa_{\text{transl},80}M_{80} - (\gamma_{G_{80}}+\mu_G)G_{80}, \\ G_{80d} = \dfrac{G_{80}^2}{\kappa_D}, \\ D_1 = \dfrac{G_{80d}D}{\kappa_A} = \dfrac{G_{80}^2 D}{\kappa_A\kappa_D}, \\ D_2 = \dfrac{(G_3^*)^2 D_1}{\kappa_B} = \dfrac{G_{80}^2(G_3^*)^2 D}{\kappa_A\kappa_B\kappa_D}, \\ [G_3^* : G_{80}] = \sqrt{\dfrac{(G_3^*)^2 G_{80d}}{\kappa_C}} = \dfrac{G_3^* G_{80}}{\sqrt{\kappa_C\kappa_D}}, \end{cases} \tag{32}$$

where

$$F_1(G_3^*,G_{80}) = 1 - \frac{1}{1+\frac{\kappa_A\kappa_D}{G_{80}^2}+\frac{(G_3^*)^2}{\kappa_B}}$$

$$\overline{K} := \frac{\kappa_{\text{cat}}}{\gamma_{G_3}+\mu_G}. \tag{33}$$

4.2. Bifurcation of the non-dissociation model

In this section we discuss how the model parameters determine which of the two possibilities (monostable versus bistable) in Case I will appear.

As mentioned in the previous section, the solution of the steady state equations (24) leads to either (27) or (28). Let us focus on system (28) with F_1 given by (31). Substituting G_3 as a function of G_{80} in (31), we obtain the fraction of the actively transcribing cells as a function of G_{80} only

$$F_1(G_3,G_{80}) = F_1(G_{80}) = 1 - \frac{1}{1+\frac{\kappa_A\kappa_D}{G_{80}^2}+X\left(\frac{B}{A}\right)^2 G_{80}^2}. \tag{34}$$

X is a combination of model paraments and is defined as $X := \overline{K}^2/\kappa_B(G_{\text{int}}/(G_{\text{int}}+K_S))^2$.

To reduce the number of parameters and to make the analysis easier, we work with a dimensionless expression for F_1. Define the dimensionless variables $g_{80} := BG_{80}, q := \kappa_A\kappa_D B^2, p := X/A^2$. Then F_1 can be rewritten as

$$F_1(g_{80}) = 1 - \frac{1}{1+\frac{q}{g_{80}^2}+pg_{80}^2} = \frac{q+pg_{80}^4}{q+g_{80}^2+pg_{80}^4}. \tag{35}$$

Therefore the protein steady state equation (28) is equivalent to

$$\begin{aligned} BG_{80} = F_1(G_{80}) &\Leftrightarrow g_{80} = F_1(g_{80}) \Leftrightarrow g_{80} = \frac{q+pg_{80}^4}{q+g_{80}^2+pg_{80}^4} \\ &\Leftrightarrow pg_{80}^5 - pg_{80}^4 + g_{80}^3 + qg_{80} - q = 0. \end{aligned} \tag{36}$$

Eq. (36) is easily found to have either one or three positive roots for g_{80} using Descartes' rule of signs. As expected on biological grounds, (36) has no negative roots. The results from Appendix E detail the nature of the stability of these steady states. Inside the cusp like region there are two locally stable positive solutions to (36), while outside that region there is but a single globally stable positive solution. This completes the demonstration of the existence of the monostable versus bistable regimes. The resulting bifurcation diagram is shown in Fig. 3.

5. *Non-dissociation model* behavior

In this section we compare the predictions from the *non-dissociation hypothesis* model with two published experimental results.

5.1. Bifurcation behavior

First we examine how the mathematical model explains the bifurcation behavior of the GAL wild type and mutants from Acar et al. (2005). In Section 2.2 we described the general experimental set up of this study. Briefly, they grew the yeast cells either in raffinose alone or raffinose and 2% galactose, and then challenged the mutant and the wild type strains with various galactose concentrations. After the strains reached a steady state, the dynamic performance was quantified through GFP expression driven by the GAL1 promoter using flow cytometry. Each of the mutant strains *gal2Δ*, *gal3Δ*, and *gal80Δ* had been engineered by replacing the endogenous promoter controlling the targeted gene (GAL2, GAL3, and GAL80, respectively) with a doxycycline-inducible promoter. By adjusting the concentration of doxycycline, the targeted genes were expressed constitutively at a level comparable to the wild type counterpart induced by 0.5% galactose.

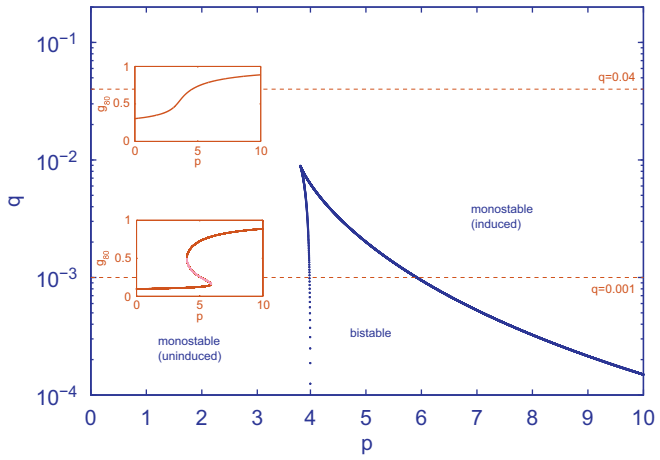

Fig. 3. The bifurcation diagram of the *non-dissociation model*. p and q are dimensionless variables related to the synthesis rate of Gal3p and Gal80p, respectively. More precisely, $p \propto (\kappa_{\text{transl},3} \cdot \kappa_{\text{transc},3})^2$ and $q \propto (\kappa_{\text{transl},80} \cdot \kappa_{\text{transc},80})^{-2}$. The parameter p is an increasing function of internal galactose concentration. Saddle node bifurcations occur along the curves separating the bistable and the monostable regimes except at the cusp point. The cusp point occurs at (3.81, 0.0089), and it involves a codimension-2 bifurcation. The insets illustrate the model steady state dependence on p when q is fixed. A situation as the one illustrated for $q=0.04$ corresponds to a gradually increasing response to galactose. In the example for $q=0.001$, the circuit is capable of residing in multiple expression states. The light colored portion of the curve shows the unstable steady states, while the dark colored portion corresponds to the locally or globally stable steady states.

To review, in the previous section we defined two non-dimensional variables

$$q := \kappa_A \kappa_D B^2 = \kappa_A \kappa_D \frac{(\gamma_{M_{80}} + \mu_M)^2 (\gamma_{G_{80}} + \mu_G)^2}{\kappa^2_{\text{transl},80} \kappa^2_{\text{transc},80}},$$

$$p := \frac{X}{A^2} = \frac{1}{\kappa_B} \left(\frac{\kappa_{\text{cat}}}{\gamma_{G_3} + \mu_G} \cdot \frac{G_{\text{int}}}{G_{\text{int}} + K_S} \cdot \frac{\kappa_{\text{transl},3} \kappa_{\text{transc},3}}{(\gamma_{M_3} + \mu_M)\left(\gamma_{G_3} + \mu_G + \kappa_{\text{cat}} \frac{G_{\text{int}}}{K_S + G_{\text{int}}}\right)} \right)^2.$$

p is an increasing function of G_{int}, and variations in p and q reflect changes in Gal3p and Gal80p synthesis, respectively (see Fig. 3). Precisely, $p \propto (\kappa_{\text{transl},3} \cdot \kappa_{\text{transc},3})^2$ and $q \propto (\kappa_{\text{transl},80} \cdot \kappa_{\text{transc},80})^{-2}$. Our mathematical formulation of the *non-dissociation model* reproduces the wild type as well as *gal3Δ* and *gal80Δ* strains characteristics in terms of the response to galactose induction. As the galactose concentration increases, p increases as well, and the GAL regulon can lie either in a bistable or a monostable region according to the values of q. If q is below the cusp q-coordinate the systems pass from uninduced monostable, to bistable, and ultimately back to an induced monostable state with increasing values of p.

The levels of Gal3p and Gal80p influence the size of the bistable region. As the concentration of Gal80p decreases (which is equivalent to an increase in q) the bistable region grows smaller. A *gal80Δ* mutant is equivalent to a fixed q value in our bifurcation diagram. A *gal3Δ* mutant corresponds to a fixed p. As in Acar et al. (2005), cells with Gal3p expressed at levels such that p is lower than the p-coordinate of the cusp point are not able to display a bimodal expression pattern. Our model does not include the synthesis of Gal2p. Therefore we cannot directly compare the model behavior for constitutive Gal2p expression with the *gal2Δ* mutant from Acar et al. (2005). However, Gal2p is the galactose permease, and is not involved directly in the regulatory mechanism. We would expect that a lower GAL2 expression would influence only the speed of GAL gene response, and not the capacity of displaying multiple steady states.

5.2. Fraction of ON cells in the model and the data

Finally, we examined the experimental data from Acar et al. (2010). In this study, the cells were pre-grown in 2% raffinose, and then exposed to 0.1% glucose and various concentrations of galactose. Their aim was to investigate the effect of the number of gene copies on the GAL network activity, and the fraction of the ON cells was considered as a quantitative phenotypic trait. Consequently, the fraction of the actively transcribing cells was measured for varying concentrations of galactose between 0.001% and 1% (w/v). The measurements were carried out at steady state for wild type strains (haploid and diploid), and heterozygous mutants GAL3$^{(+/-)}$, GAL80$^{(+/-)}$, GAL4$^{(+/-)}$, GAL2$^{(+/-)}$.

We focused on the inducibility profiles of the diploid wild type, and of the GAL3$^{(+/-)}$ and GAL80$^{(+/-)}$ mutant strains, limiting our study to a qualitative comparison for two reasons. First, the fraction of the actively transcribing cells (F_1) in our model is a function of the internal galactose concentration, and data were collected with respect to the external galactose concentration. We have no additional experimental measurements to help us connect the external and the internal galactose concentration in a cell. Second, Acar et al. (2010) employ GFP expression driven by a promoter with four binding sites (GAL1) which has no basal level of expression. On the other hand, our model describes the GAL dynamics driven by GAL3 and GAL80 promoters. Both of them have a single binding site for Gal4p dimers and a leaky expression. Fig. 4 is a qualitative comparison between the fraction of actively transcribing cells in our model F_1 given by (33) and the experimental data from Acar et al. (2010, Fig. 2B). The predicted and the measured fraction of the ON cells for the wild type strain have the same qualitative behavior. Similarly for the GAL3$^{(+/-)}$ heterozygous mutant.When decreasing the number of GAL3 genes being expressed, our model simulations show that the GAL genes require a higher concentration of galactose to become induced. There is a high degree of similarity between the model and the data in the case of GAL80$^{(+/-)}$ cells as well. When decreasing the number of GAL80 genes being expressed, our model predicts that the basal level of expression will increase, and consequently, a larger fraction of cells will be induced at low sugar concentration. In comparison to the wild type strain, the GAL80$^{(+/-)}$ strain requires a lower concentration of galactose to reach half of the maximal induction level. These predictions are reasonable given that GAL80 is the repressor which inhibits the expression of the GAL genes in the absence of galactose.

5.3. Non-dissociation model predictions: binary versus graded response to galactose induction

An intriguing question is whether the gene transcription is initiated due to a switch between inactive and active states or through a gradual and smoothly increasing cell response. The former is a hallmark of the bistable or the binary behavior, and the latter of the graded response. The majority of the existing evidence suggests that within a single cell, the GAL genes are either fully induced or not induced at all in the presence of galactose. However, a few studies have shown contradictory findings.

For example, the *gal2Δ S. cerevisiae* cells from Acar et al. (2005) responded in a binary fashion to galactose induction, while the *gal2Δ S. cerevisiae* strain from Hawkins and Smolke (2006, Fig. 5) displayed a graded response pattern. We do not model GAL2 time evolution, but our qualitative predictions are still valid for a *gal2Δ* mutant. GAL2 encodes for the galactose permease and mediates the sugar transport across the nuclear membrane. A decrease in

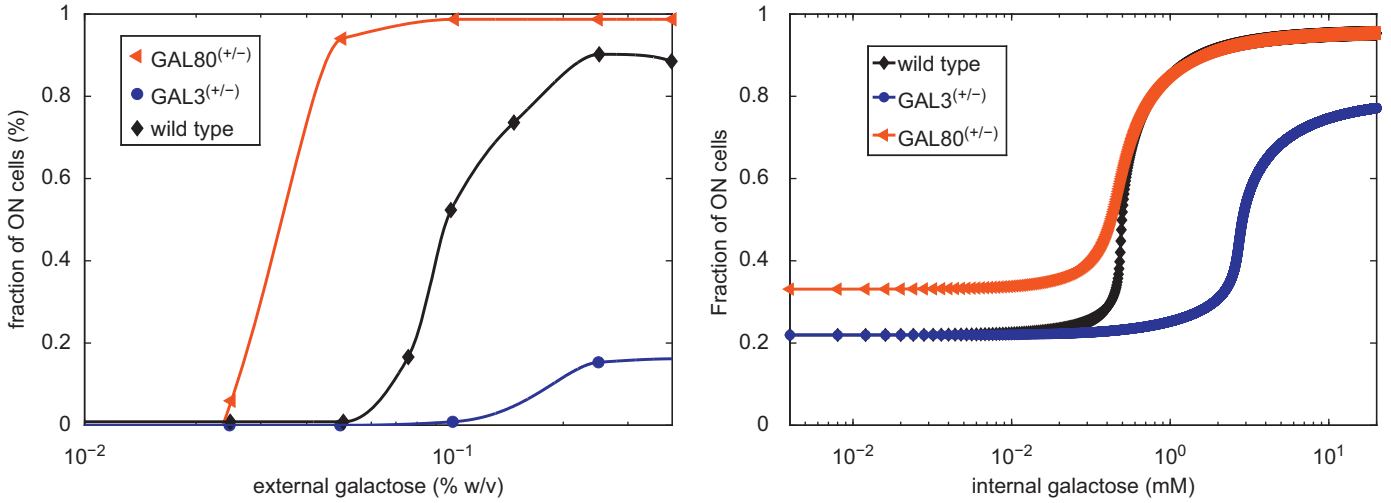

Fig. 4. Qualitative comparison between the fraction of actively transcribing cells in our model F_1 given by (33), and the experimental data from Acar et al. (2010, Fig. 2B). The reason of the *apparent* discrepancy in basal level of expression between the data and the model is due to the different GAL promoters involved. Precisely, Acar et al. (2010) employ GFP expression driven by a promoter with four binding sites (GAL1) which has no basal level of expression (no leakage). Our model describes the GAL dynamics driven by GAL3 and GAL80 promoters which have a single binding site for Gal4p dimers and a leaky expression. Left panel: data set published by Acar et al. (2010). Right panel: fraction of ON cells F_1 in our model as a function of internal galactose concentration.To simulate a heterozygous strain we reduced by half the mRNA synthesis rate of the wild type strain. The black curve corresponds to F_1 for wild type cells, and the blue curve shows the changes in F_1 for a GAL3$^{(+/-)}$ heterozygous mutant. The red curve illustrates the function F_1 for GAL80$^{(+/-)}$ cells. (For interpretation of the references to color in this figure legend, the reader is referred to the web version of this article.)

Gal2p protein numbers does not affect the regulatory mechanism but will slow down the speed of galactose import. The experimental data from Acar et al. (2010, Fig. 2C) shows that a heterozygous mutant GAL2$^{(+/-)}$ has the same induction profile as the wild type except that cells need a slightly higher concentration of external galactose to be induced.

Biggar and Crabtree (2001) raised the question of binary versus graded response when studying the GAL circuit in yeast cells challenged with glucose. The same yeast strain had either two distinct states at intermediate concentrations of glucose when pre-grown in glucose, or a gradual increase in GAL1–GFP when pre-grown on raffinose. The model bifurcation diagram shown in Fig. 3 suggests that theoretically, the GAL network of the same yeast strain is able to display both graded and binary behavior in response to the inducer. The two insets illustrate this idea. When galactose increases (which implies that p increases as well), and q is above the q-coordinate of the cusp point, the system smoothly changes from monostable uninduced to monostable induced, *i.e.* it has a graded behavior. If q is under the q-coordinate of the cusp point then the system traverses the monostable uninduced, bistable, and then the monostable induced regimes. According to our study, the appearance of a graded versus binary response is dependent on many factors. It is likely that the experimental set-up, the pre-growth history, and implicitly the initial state of the cells before addition of galactose may be among the factors that can influence the fate of the cell population after induction.

6. Discussion

In this paper, we have proposed a mathematical framework for the GAL regulon induction in a large population of *S. cerevisiae* cells, taking into consideration the most recent experimental findings (Wightman et al., 2008; Jiang et al., 2009). Although the budding yeast and the GAL genes have been studied at biochemical and genetic level for a few decades, many questions are still left unanswered. Presently, it is not completely understood either how the galactose signal is sensed by the transcriptional machinery or the fate of the complex formed by Gal80p and galactose-activated Gal3p. The interaction between Gal80p and galactose-activated Gal3p is believed to be the key factor which somehow reliefs the repression at the promoters, and allows the GAL genes transcription to be initiated. For the latter aspect, two contradictory models have been proposed in the literature. Both the *non-dissociation* and the *dissociation model* have been presented in Section 2.1, and graphically illustrated in Fig. 1. In our mathematical study we used quantitative tools to distinguish between the *non-dissociation* and the *dissociation hypotheses* at GAL promoters, and assessed which of them might explain the fundamental properties of the network noted experimentally.

We choose the bistable character of the GAL circuit displayed by the wild type cell populations (Hawkins and Smolke, 2006; Song et al., 2010; Acar et al., 2005, 2010) as the main system characteristic to compare the *non-dissociation* and the *dissociation hypotheses*. Given the current understanding of the GAL regulon underlying biology on which our model was build on (Wightman et al., 2008; Jiang et al., 2009), our study brings support to the idea that the *non-dissociation theory* is the most likely mechanism leading to distinct expression states at intermediate concentration of galactose. Our deterministic model captures the key proteins synthesis and the essential interaction between them.

Additionally, we considered all the fast processes at steady state (e.g., Gal80p dimerization, dissociation of the complex formed by Gal80p and activated Gal3p). Despite the simplifying assumptions, the model we propose reproduces quantitatively the experimental flow cytometry histograms of the wild type, *gal*3Δ, and *gal*80Δ mutant cells published in Acar et al. (2005). Moreover, our model employs a fraction of actively transcribing cells which has the same qualitative features as in the data set collected by Acar et al. (2010). There is a good agreement between the model and the data for the wild type and GAL3$^{(+/-)}$ heterozygous mutant cells, and a high degree of similarity in the case of GAL80$^{(+/-)}$ strain. To our knowledge, our model is the first to capture the dynamic interplay of the key proteins governing the induction process, and to reproduce the bistable network behavior found experimentally. The mathematical study from Acar

et al. (2005) shows bistability but it describes the changes in the total concentration of Gal3p in a strain disabled for GAL80 autoregulation.

We had to limit the model validation to a qualitative comparison due to the lack of additional experimental measurements to help us identify key parameter values like the Michaelis–Menten constant (K_S) and the catalytic constant (κ_{cat}) for Gal3p activation by galactose. In Appendix C we propose a full parameter estimation scheme given that K_S, κ_{cat}, and κ_C (the dissociation constant of the complex formed by Gal80p and activated Gal3p) are known. To investigate the model behavior, we chose physiologically relevant values for the three parameters, a GAL80 transcription rate such that the model is placed in a parameter region with the potential of leading to bistability, and then followed the parameter estimation scheme presented in Appendix C.

In our work, we consider a large population of cells. If one is interested in GAL regulon dynamics upon galactose challenge in single cells then the bursting dynamics and the likelihood of noise in parameters should be taken into consideration (Mackey et al., 2011).

From our perspective, the mathematical model presented in this paper leads to interesting predictions. In Section 5.3 we addressed the question of debate regarding the binary versus the graded *S. cerevisiae* cell response to galactose induction. The result was surprising. The mathematical model built on the *non-dissociation theory* reveals that theoretically, both graded and binary responses are possible for the same strain. This is exactly what Biggar and Crabtree (2001) noticed experimentally when challenging with glucose the same *S. cerevisiae* strain. Also, different behaviors were observed in the case of *gal2Δ* cells in response to galactose. Acar et al. (2005) report a binary response pattern, while Hawkins and Smolke (2006) a graded induction.

The current model can be used for other predictions as well. For example, it can be used to test hypotheses regarding the yeast cells transcriptional memory. Kundu and Peterson (2010) proposes that the fast induction kinetics of cells with an *a priori* exposure to galactose might be due to the GAL proteins already present in the cell and not degraded through dilution. This quantitative test would require the inclusion of cell division in modeling GAL regulon dynamics. Another appealing idea is to couple the genetic component modeled in this paper with the Leloir pathway which converts galactose into a more metabolically efficient sugar, and see how they influence each other. One of the applications of the extended model would be to analyze the consequences of the impairment of the Leloir enzymes (GAL1, GAL7, GAL10). The Leloir enzymes impairment is the cause of a human recessive disorder called galactosemia (Mumma et al., 2008).

Acknowledgments

This work was supported by Mathematics of Information Technology and Complex Systems (MITACS, Canada) and Natural Sciences and Engineering Research Council of Canada (NSERC, Canada). R.A. would like to thank Alina Ilie, Romain Yvinec, Changjing Zhuge, and Lennart Hilbert for useful comments and suggestions.

Appendix A. *Non-dissociation model*: fraction of cells with two UASg at GAL promoters which are actively transcribing in the presence of galactose

Our study shows that the *non-dissociation model* may confer the GAL network a bistable behavior which is robust to variations in the parameter values as well as to the number of UASg for the Gal4p homodimers. For example, let us consider a GAL promoter with two binding sites, and with G_3^* monomers binding simultaneous at each site, *i.e.*

$$\begin{cases} 2G_{80} \rightleftharpoons^{\kappa_D} G_{80d}, \\ 2G_{80d} + D' \rightleftharpoons^{\overline{\kappa}_A} D_1', \\ 2G_3^* + D_1' \rightleftharpoons^{\overline{\kappa}_B} D_2', \\ 2G_3^* + D_2' \rightleftharpoons^{\overline{\kappa}_B} D_3', \end{cases} \tag{A.1}$$

where

$$D' := [\text{UASg} : 2G_{4d}], \tag{A.2}$$

$$D_1' := [\text{UASg} : 2G_{4d} : 2G_{80d}] = [D' : 2G_{80d}], \tag{A.3}$$

$$D_2' := [\text{UASg} : 2G_{4d} : 2G_{80d} : 2G_3^*] = [D_1' : 2G_3^*], \tag{A.4}$$

$$D_3' := [\text{UASg} : 2G_{4d} : 2G_{80d} : 2G_3^* : 2G_3^*] = [D_2' : 2G_3^*]. \tag{A.5}$$

At equilibrium, from (A.1) we have

$$\kappa_D = \frac{G_{80}^2}{G_{80d}} \Rightarrow G_{80d} = \frac{G_{80}^2}{\kappa_D},$$

$$\overline{\kappa}_A = \frac{D' \cdot G_{80d}}{D_1'} \Rightarrow D' = \frac{\overline{\kappa}_A \kappa_D}{G_{80}^2} D_1',$$

$$\overline{\kappa}_B = \frac{(G_3^*)^2 D_1'}{D_2'} \Rightarrow D_2' = \frac{(G_3^*)^2}{\overline{\kappa}_B} D_1',$$

$$\overline{\kappa}_B' = \frac{(G_3^*)^2 D_2'}{D_3'} \Rightarrow D_3' = \frac{(G_3^*)^4}{\overline{\kappa}_B \overline{\kappa}_B'} D_1'.$$

The total concentration of the promoter is $D_T = D' + D_1' + D_2' + D_3'$, and the only promoter configurations leading to transcription are D', D_2', and D_3'. Therefore

$$\begin{aligned} F_2(G_3^*, G_{80}) = \frac{D' + D_2' + D_3'}{D_T} &= \frac{\frac{\overline{\kappa}_A}{G_{80}^2} D_1' + \frac{(G_3^*)^2}{\overline{\kappa}_B} D_1' + \frac{(G_3^*)^4}{\overline{\kappa}_B \overline{\kappa}_B'} D_1'}{D_1' + \frac{\overline{\kappa}_A}{G_{80}^2} D_1' + \frac{(G_3^*)^2}{\overline{\kappa}_B} D_1' + \frac{(G_3^*)^4}{\overline{\kappa}_B \overline{\kappa}_B'} D_1'} \\ &= \frac{\frac{\overline{\kappa}_A}{G_{80}^2} + \frac{(G_3^*)^2}{\overline{\kappa}_B} + \frac{(G_3^*)^4}{\overline{\kappa}_B \overline{\kappa}_B'}}{1 + \frac{\overline{\kappa}_A}{G_{80}^2} + \frac{(G_3^*)^2}{\overline{\kappa}_B} + \frac{(G_3^*)^4}{\overline{\kappa}_B \overline{\kappa}_B'}} = 1 - \frac{1}{1 + \frac{\overline{\kappa}_A}{G_{80}^2} + \frac{(G_3^*)^2}{\overline{\kappa}_B} + \frac{(G_3^*)^4}{\overline{\kappa}_B \overline{\kappa}_B'}}. \end{aligned} \tag{A.6}$$

Since at steady state, from Eq. (23)

$$G_3^* = \overline{K} \frac{G_3 G_{\text{int}}}{G_{\text{int}} + K_S},$$

it follows that at steady state F_2 depends on G_3, G_{80}, G_{int}. Hence

$$\begin{aligned} F_2(G_3, G_{80}, G_{\text{int}}) &= 1 - \frac{1}{1 + \frac{\overline{\kappa}_A}{G_{80}^2} + \frac{(G_3^*)^2}{\overline{\kappa}_B} + \frac{(G_3^*)^4}{\overline{\kappa}_B \overline{\kappa}_B'}} \\ &= 1 - \frac{1}{1 + \frac{\overline{\kappa}_A}{G_{80}^2} + \frac{(G_3)^2}{\overline{\kappa}_B} \left(\frac{\overline{K} G_{\text{int}}}{G_{\text{int}} + K_S} \right)^2 + \frac{(G_3)^4}{\overline{\kappa}_B \overline{\kappa}_B'} \left(\frac{\overline{K} G_{\text{int}}}{G_{\text{int}} + K_S} \right)^4}. \end{aligned} \tag{A.7}$$

Appendix B. *Dissociation model*: fraction of cells with one UASg at GAL promoters which are actively transcribing in the presence of galactose

The fraction of the ON cells in the case of *dissociation model* is treated similarly as in Section 3.1.1 and Appendix A. Let us consider a GAL promoter with one binding site. Gal4p dimers are tethered at UASg with Gal80p dimers blocking their activation domains in the absence of galactose. Simultaneous binding of G_3^*

monomers to [UASg : G_{4d} : G_{80d}] removes the repressor and allows the transcription to be initiated. This series of events are summarized by the following set of chemical reactions:

$$\begin{cases} 2G_{80} \rightleftharpoons^{\kappa_D} G_{80d}, \\ D + G_{80d} \rightleftharpoons^{\kappa_A} [D : G_{80d}], \\ 2G_3^* + [D : G_{80d}] \rightleftharpoons^{\kappa_B} D + 2[G_3^* : G_{80}], \end{cases} \tag{B.1}$$

where

$$D := [\text{UASg} : G_{4d}], \tag{B.2}$$

$$D_1 := [\text{UASg} : G_{4d} : G_{80d}] = [D : G_{80d}]. \tag{B.3}$$

κ_A, κ_B, κ_D are dissociation constants. At equilibrium, from (B.1) we have

$$\kappa_D = \frac{G_{80}^2}{G_{80d}} \Rightarrow G_{80d} = \frac{G_{80}^2}{\kappa_D},$$

$$\kappa_A = \frac{D \cdot G_{80d}}{D_1} \Rightarrow D_1 = \frac{G_{80}^2}{\kappa_A \kappa_D} D,$$

$$\kappa_B = \frac{(G_3^*)^2 \cdot D_1}{D \cdot [G_3^* : G_{80}]^2} \Rightarrow D_1 = \kappa_B \frac{[G_3^* : G_{80}]^2}{(G_3^*)^2} D.$$

The total concentration of the promoter is $D_T = D + D_1$. The transcriptional machinery can be recruited at the promoter only when it is in configuration D. Hence

$$F_1 = \frac{D}{D_T} = \frac{1}{1 + \kappa_B \frac{[G_3^* : G_{80}]^2}{(G_3^*)^2}} = \frac{1}{1 + \frac{G_{80}^2}{\kappa_A \kappa_D}}.$$

Appendix C. Parameter estimation

One the most daunting tasks of modeling is the estimation of the parameters. The literature on the GAL system contains a collection of independent experiments involving different strains of yeast, and different experimental set-ups with various carbon sources used for cell growth (see Table C2). This information is sufficient to provide an estimation of 12 out of the 16 model parameters. In this section we summarize our findings for these parameters obtained by combining the experimental measurements with the mathematical relations dictated by our model.

- κ_r. As in Venkatesh et al. (1999), we assume that all Gal3p is activated in the presence of the inducing sugar, *i.e.* κ_r in reaction (18) is negligible.
- mRNA and protein degradation rates. As the study of Bennett et al. (2008) shows, it is very likely that the GAL mRNAs and proteins have a carbon-dependent degradation rate. Since most of the measurements found in the literature are turnover rates in a glucose-rich medium, we had to consider these values for the case of galactose as well (see Table C2). Due to lack of experimental information on Gal3p activation by galactose we assume that Gal3p* has the same degradation rate as Gal3p (*i.e.*, $\gamma_{G_3^*} = \gamma_{G_3}$).
- Dilution rate. The dilution rate has been previously estimated as 3.85×10^{-3} min^{-1} based on a yeast doubling time of 180 minutes (Ramsey et al., 2006).
- mRNA steady state levels. To estimate the number of mRNA molecules for uninduced and fully induced states we combined the experimental measurements from several studies. Arava et al. (2003) estimated 0.9 and 1.2 mRNA molecules/cell for GAL3 and GAL80, respectively under glucose repression. Under the same carbon source Holstege et al. (1998) found 0.8 GAL80 molecules/cell. Lashkari et al. (1997) measured the change in gene expression when cells are switched from glucose to galactose medium and noticed a 8.6 and 3 fold increase for GAL3 and GAL80, respectively. Therefore, we deduce that there are 7.74 GAL3 molecules/cell and 3.36–3.6 GAL80 molecules/cell. Ideker et al. (2001) applied genetic and environmental perturbations to the GAL pathway, and looked at the global changes in mRNA expression resulting from each perturbation. When comparing the wild type cells grown in 2% raffinose with or without 2% galactose they noticed a 2.041 and 3.23 fold increase in galactose versus raffinose in GAL3 and GAL80 gene expression, respectively. This allowed us to infer the levels of GAL3 and GAL80 mRNAs in raffinose as 3.79 molecules/cell and 1.04–1.11 molecules/cell, respectively.
- κ_B, κ_A, κ_D. All these parameters have been measured and published by different laboratories. See Table C2 for the corresponding values and sources.
- Steady state levels of the complex $D = [\text{UASg} : G_{4d}]$. By considering a promoter with one binding site for Gal4p as one molecule with one binding site for this protein, and a yeast cell volume of 70 μm^3 (Bhat, 2008), we obtain $D = 4.7 \times 10^{-8}$ mM.
- Protein steady state levels in raffinose. Ghaemmaghami et al. (2003) performed a genome-wide study and measured *S. cerevisiae* proteins levels in cells fed with glucose. Their study shows that there are 721 Gal3p and 784 Gal80p under glucose repression. For modeling purposes, we assumed the same translational efficiency in non-repressing non-inducing conditions (e.g., raffinose) as in glucose. Therefore we have

Table C1
Model steady state values calculated from experimental data. Our model captures the GAL molecular switch from non-inducing non-repressing sugars (*e.g.*, raffinose) to galactose. The column with experimentally measured values in glucose is introduced for comparison purposes. The dagger (†) denotes that the 784 Gal80p protein number includes the numbers of free monomers and dimers, as well as the [UASg : G_{4d}]-bound dimers. Source of the experimental measurements: Arava et al. (2003) and Holstege et al. (1998) for the mRNA levels in glucose, Ghaemmaghami et al. (2003) for the protein levels in glucose. The conversion between mM and molecules/cell assumes a yeast cell volume of 70 μm^3 (Bhat, 2008). NE stands for "not estimated".

Model variable	Notation	Value			Unit
		Glucose (experimental)	Raffinose (calculated)	Galactose (calculated)	
GAL3 mRNA	M_3	0.9	3.79	7.74	Copies/cell
Gal3p protein	G_3	721	3036.2	NE	Proteins/cell
Activated Gal3p	G_3^*	0	0	NE	Proteins/cell
GAL80 mRNA	M_{80}	1.2	1.11	3.6	Copies/cell
Gal80p protein	G_{80}	784†	89.69	NE	Proteins/cell
Gal80p dimer	G_{80d}	–	631.41	NE	Proteins/cell
Complex of G_3^* and G_{80}	$[G_3^* : G_{80}]$	0	0	NE	Proteins/cell
[UASg : G_{4d}]	D	–	4.7×10^{-8}	4.7×10^{-8}	mM
[UASg : G_{4d} : G_{80d}]	D_1	–	14.19×10^{-8}	NE	mM
[UASg : G_{4d} : $2G_3^*$]	D_2	0	0	NE	mM

Table C2
Model parameters (all except for κ_{cat}, K_S, κ_C). YPD (yeast extract/peptone/dextrose) is a growth medium rich in glucose for growing yeast cells. The protein and mRNA degradation values taken from [4] include both the degradation intrinsic factors and the dilution. In our modeling, we assume that the galactose-bound form of Gal3p has the same degradation as Gal3p, and we consider the reverse rate κ_r as negligible. Sources: [1]=Arava et al. (2003), [2]=Melcher and Xu (2001), [3]=Bennett et al. (2008), [4]=Ramsey et al. (2006), [5]=Acar et al. (2005), [6]=Lohr et al. (1995), [7]=Holstege et al. (1998), [8]=Belle et al. (2006).

Model parameters	Parameter	Experimental value	Model value	Unit	Source
mRNA degradation rates	γ_{M_3}	26.6×10^{-3}		min^{-1}	[4]
		$\frac{\ln 2}{16}=43.32\times10^{-3}$ (galactose)	43.32×10^{-3}	min^{-1}	[3]
	$\gamma_{M_{80}}$	$\frac{\ln 2}{16}=43.32\times10^{-3}$ (YPD)	43.32×10^{-3}	min^{-1}	[7]
		28.88×10^{-3}		min^{-1}	[4]
mRNA dilution rate	μ_M	–	3.85×10^{-3}	min^{-1}	[4]
Transcription rates	$\kappa_{transcr,3}$	–	0.365	Molecules/min	Calculated
	$\kappa_{transcr,80}$	1.8 (YPD-[7])	0.169	Molecules/min	Calculated
Protein degradation rates	γ_{G_3}	11.55×10^{-3}	11.55×10^{-3}	min^{-1}	[4]
		$\frac{\ln 2}{18}=38.5\times10^{-3}$ (YPD)		min^{-1}	[8]
	$\gamma_{G_{80}}$	6.93×10^{-3}	6.93×10^{-3}	min^{-1}	[4]
		$\frac{\ln 2}{2856}=0.24\times10^{-3}$ (YPD)		min^{-1}	[8]
Protein dilution rate	μ_G	–	$\frac{\ln 2}{180}=3.85\times10^{-3}$	min^{-1}	[4]
protein synthesis rates	$\kappa_{transl,3}$	2.4 (YPD-[1])		(Proteins/mRNA)/min	Calculated
	$\kappa_{transl,80}$	1.2 (YPD-[1])		(Proteins/mRNA)/min	Calculated
dissociation constants	κ_B	6×10^{-8}	6×10^{-8}	mM^2	[5]
	κ_D	$1–3\times10^{-7}$ ([2])	3×10^{-7}	mM	Calculated
	κ_A	5×10^{-6} ([6])	5×10^{-6}	mM	Calculated
		3×10^{-8} ([2])		mM	

3036.2 Gal3p and 725.2 Gal80p proteins in raffinose. The 725.2 Gal80p molecules sum up the number of free monomers, free dimers and Gal4p-bound dimers

$$[G_{80}]_{\text{total}}^{\text{raffinose}} = G_{80}+G_{80d}+D_1 = 725.2 \quad \text{molecules.}$$

Using the relations (32) we can write

$$[G_{80}]_{\text{total}}^{\text{raffinose}} = G_{80}+G_{80d}+D_1 = G_{80}+\frac{G_{80}^2}{\kappa_D}+\frac{G_{80}^2}{\kappa_A\kappa_D}D = 725.2 \text{ molecules.}$$

This implies $G_{80}=89.69$ molecules and $G_{80d}=636.41$ molecules.

- Basal mRNA level of expression (leakage) in our model. The GAL genes whose expression is driven by promoters with a single UASg have a basal level β in the absence of galactose (Melcher and Xu, 2001). In our model, the leakage expression corresponds to F_1 when $G_{\text{int}}=0$

$$\beta = F_1(G_3,G_{80},G_{\text{int}}=0) = 1-\frac{1}{1+\frac{\kappa_A\kappa_D}{G_{80}^2}} = 0.24.$$

Ruhela et al. (2004) measured the protein levels of α-galactosidase from MEL1, which is a structural GAL gene with one binding site for Gal4p, and noticed a minimum of 5%–10% protein in the absence of galactose.

- Steady state levels of the DNA-bound complexes D_1 and D_2 in raffinose. $D_1=(G_{80}^2/\kappa_A\kappa_D)D=14.19\times10^{-8}$ mM and $D_2=0$ mM.
- Transcription rates. For simplicity, we consider that GAL3 and GAL80 genes are transcribed at the same rate when the galactose is supplied to the medium regardless of its concentration. The data sets from Acar et al. (2010), Fig. 2 presents the fraction of actively transcribing cells (F_1) reaching 100% at saturating concentrations of galactose. Therefore

$$\kappa_{\text{transcr,i}} = M_i\frac{\gamma_{M_i}+\mu_M}{100\%}, \quad i\in\{3,80\}.$$

Consequently, we obtain transcription rates of 0.365 molecules/min and 0.169 molecules/min for GAL3 and GAL80, respectively. Holstege et al. (1998) estimated that 1.8 GAL80 mRNA molecules are transcribed per cell per minute in a glucose-rich medium, value which is about one order of magnitude higher than our estimation. There are at least three possible explanations for this difference. It is possible the repressor GAL80 to be transcribed at a lower rate in galactose than in glucose, GAL80 mRNA to have a sugar dependent degradation rate as Bennett et al. (2008) mentioned that it might be the case in the GAL circuit, and the estimated mRNA levels in galactose to be imprecise due to sequence of measurements used for their inference.

Parameters left unestimated: We did not find any information in the literature about the activation of Gal3p by galactose and the protein steady state levels at any concentration of galactose. Since we had no access to any experimental data sets except the ones from Acar et al. (2005, 2010) we had no means of estimating κ_{cat}, K_S, κ_C, $\kappa_{transl,3}$, $\kappa_{transl,80}$, and the proteins/complexes steady states in galactose-induced cells. We gathered some information which can be used in tandem with the mathematical relations derived from our model. In the following, we propose a complete scheme to estimate all the remaining parameters given that κ_{cat}, K_S, and κ_C are known. From our perspective, κ_{cat} are K_S key parameters for the cellular components time evolution and steady state levels.

- Protein steady state levels at saturating concentrations of galactose. Due to the lack of additional information on Gal3p and Gal80p molecule numbers in the induced state, we use some average estimates. Ghaemmaghami et al. (2003) examined the relationship between the protein and mRNA levels. Although individual genes with similar mRNA levels can result in a wide spectrum of protein abundance, on average, the mRNA to protein level ratio per cell is constant. This ratio varies among MIPS functional categories or the localization categories. Overall, it was estimated a ratio of protein per mRNA of either 4800 or 4200 depending on the abundance measurement. As in Ghaemmaghami et al. (2003) we consider an average ratio of 4,800 protein per mRNA per cell. Consequently, we assume a total of 37,150 Gal3p per cell under saturating galactose

concentrations ($[G_3]_{\text{total}} = 37,150$ proteins). Since the Gal3p concentration is five times greater than the total concentration of Gal80p at full induction (Bhat, 2008) it follows that $[G_{80}]_{\text{total}} = 7,450$ proteins

$$[G_3]_{\text{total}} = G_3 + G_3^* + [G_3^* : G_{80}] + 2D_2,$$

$$[G_{80}]_{\text{total}} = G_{80} + 2G_{80d} + 2D_1 + 2D_2 + [G_3^* : G_{80}].$$

Using the relations (32), we obtain

$$\begin{cases} [G_3]_{\text{total}} = G_3 + G_3^*\left(1 + \dfrac{G_{80}}{\sqrt{\kappa_C \kappa_D}}\right) \\ \quad + 2\dfrac{G_{80}^2 (G_3^*)^2 D}{\kappa_A \kappa_B \kappa_D} = 37,150 \text{ proteins} \\ [G_{80}]_{\text{total}} = G_{80} + 2\dfrac{G_{80}^2}{\kappa_D} \\ \quad + 2\dfrac{G_{80}^2 D}{\kappa_A \kappa_D} + 2\dfrac{G_{80}^2 (G_3^*)^2 D}{\kappa_A \kappa_B \kappa_D} + \dfrac{G_3^* G_{80}}{\sqrt{\kappa_C \kappa_D}} = 7450 \text{ proteins}, \end{cases} \tag{C.1}$$

where the galactose-activated Gal3p (G_3^*) at steady state is given by

$$G_3^* = \overline{K}\frac{G_3 G_{\text{int}}}{G_{\text{int}} + K_S}.$$

If κ_{cat}, K_S, κ_C was known then it would be easy to estimate G_3, G_{80} at full induction as solution of the system of two nonlinear algebraic equations (C.1).

- According to our model, the steady state levels of the DNA-bound complexes D_1 and D_2 in saturating concentrations of galactose are given by $D_1 = ((G_{80}^{\text{gal}})^2/\kappa_A\kappa_D)D$ and $D_2 = ((G_{80}^{\text{gal}})^2 (G_3^*)^2 D)/\kappa_A\kappa_B\kappa_D$, and depend directly on G_3 and G_{80} in galactose.
- Translation rates in galactose. Arava et al. (2003) estimated that 2.4 and 1.2 Gal3p and Gal80p proteins, respectively, are translated per mRNA per minute in a glucose-rich medium. Given the array of parameters collected from the literature, and the range of bistability illustrated in Fig. 3 ($3.81 < p$ and $10^{-4} < q < 10^{-2}$), a necessary condition for a strain to reside in distinct expression states is that $3.4 < \kappa_{\text{transl},80} < 34.8$ proteins/mRNA/min. Therefore we cannot use the glucose-measured value for $\kappa_{\text{transl},80}$ in our model. Instead, we estimate $\kappa_{\text{transl},80}$ using our model. At steady state, the Eqs. (32) imply that

$$\kappa_{\text{transl},80} = \frac{G_{80}}{M_{80}}(\gamma_{G_{80}} + \mu_G).$$

In our model $\kappa_{\text{transl},3}$ is galactose-dependent

$$\kappa_{\text{transl},3} = \frac{G_3}{M_3}\left(\gamma_{G_3} + \mu_G + \kappa_{\text{cat}}\frac{G_{\text{int}}}{G_{\text{int}} + K_S}\right). \tag{C.2}$$

Since γ_{G_3}, μ_G, and M_3 in galactose are already measured, $\kappa_{\text{transl},3}$ can be easily estimated. Once κ_{cat} and K_S are known, G_3 and $\kappa_{\text{transl},3}$ are straightforward to calculate from (C.1) and (C.2), respectively.

Appendix D. *Non-dissociation model* (32) in dimensionless form

We choose a dimensionless form of our model equations given by (32) in agreement with the computations from Section 4.2. By considering the non-dimensional variables

$$g_3 := AG_3,$$

$$g_3^* := AG_3^*,$$

$$m_3 := AM_3,$$

$$g_{80} := BG_{80},$$

$$m_{80} := BM_{80},$$

we can rewrite the model (32) as

$$\begin{cases} \dfrac{dm_3}{dt} = F_1(g_3^*, g_{80}, G_{\text{int}})\tilde{\kappa}_{\text{transc},3} - \tilde{\gamma}_{M_3} m_3, \\ \dfrac{dg_3}{dt} = \kappa_{\text{transl},3} m_3 - \tilde{\gamma}_{G_3} g_3 - g_3 \dfrac{\kappa_{\text{cat}}}{1 + \kappa_S}, \\ \dfrac{dg_3^*}{dt} = g_3 \dfrac{\kappa_{\text{cat}}}{1 + \kappa_S} - \tilde{\gamma}_{G_3} g_3^*, \\ \dfrac{dm_{80}}{dt} = F_1(g_3^*, g_{80})\tilde{\kappa}_{\text{transc},80} - \tilde{\gamma}_{M_{80}} m_{80}, \\ \dfrac{dg_{80}}{dt} = \kappa_{\text{transl},80} m_{80} - \tilde{\gamma}_{G_{80}} g_{80}, \end{cases} \tag{D.1}$$

where

$$\tilde{\gamma}_{M_i} := \gamma_{M_i} + \mu_M,$$

$$\tilde{\gamma}_{G_i} := \gamma_{G_i} + \mu_G,$$

$$\tilde{\kappa}_{\text{transc},3} := A\kappa_{\text{transc},3},$$

$$\tilde{\kappa}_{\text{transc},80} := B\kappa_{\text{transc},80},$$

$$\kappa_S := \frac{K_S}{G_{\text{int}}},$$

$$q := \kappa_A \kappa_D B^2.$$

The fraction of the actively transcribing cells (33) becomes

$$F_1(g_3^*, g_{80}) = 1 - \frac{1}{1 + \frac{q}{g_{80}^2} + \frac{(g_3^*)^2}{r}}, \tag{D.2}$$

where $r := A^2\kappa_B$. Note that $r = \frac{X\kappa_B}{p}$.

Appendix E. Stability analysis of the *non-dissociation model* (D.1)

The purpose of this section is to investigate the stability of the steady states of the model in its dimensionless form (D.1). Due to the nonlinearity and the high dimensionality of the model, we cannot discuss this problem in its total generality. Rather, we examine the system behavior in a small neighborhood of the fixed points or steady states and do a linear stability analysis.

Let us consider a set of autonomous ordinary differential equations, written in vector form as

$$\dot{x}(t) = f(x(t)), \tag{E.1}$$

with x^S an equilibrium point defined by $\dot{x^S}(t) = f(x^S(t)) = 0$. Let $\Delta x(t) := x(t) - x^S$ be a deviation from the steady state. We are interested to know how trajectories behave in the neighborhood of the steady state. Therefore Δx is very small, and the vector field is well approximated by the first terms in the Taylor expansion around the steady state x^S. Eq. (E.1) becomes

$$\begin{aligned} \Delta\dot{x}(t) = \dot{x}(t) = f(x(t)) &= \underbrace{f(x^S)}_{=0} + \left.\frac{\partial f}{\partial x}\right|_{x^S}(x(t) - x^S) + \frac{1}{2!}\left.\frac{\partial^2 f}{\partial x^2}\right|_{x^S}(x(t) - x^S)^2 + \cdots \\ &\approx \left.\frac{\partial f}{\partial x}\right|_{x^S}(x(t) - x^S) = \left.\frac{\partial f}{\partial x}\right|_{x^S}\Delta x(t), \end{aligned} \tag{E.2}$$

which is equivalent to

$$\Delta\dot{x}(t) = J^S \Delta x(t). \tag{E.3}$$

J^S is the constant matrix given by the Jacobian evaluated at the stationary point. Since (E.3) is a linear differential equation, its solution can be written as a superposition of terms of the form $e^{\lambda_j t}$

where $\{\lambda_j\}$ is the set of eigenvalues of the Jacobian. The complex part of $\{\lambda_j\}$ contributes to the oscillatory component of the solutions, and the real part of the eigenvalues show whether the trajectories will tend to move away or toward the stationary point x^S. Consequently, for a given set of parameters, an equilibrium point x^S of a system of ordinary differential equations (E.1) is locally stable if all the eigenvalues of the Jacobian evaluated at the equilibrium point J^S have negative real parts. If at least one of the eigenvalues has a positive real part then the equilibrium point is unstable.

For our model (D.1)

$$x(t)=\begin{bmatrix} m_3(t)\\ g_3(t)\\ g_3^*(t)\\ m_{80}(t)\\ g_{80}(t)\end{bmatrix},\quad f(x(t))=\begin{bmatrix} F_1(g_3^*(t),g_{80}(t))\tilde{\kappa}_{\text{transc},3}-\tilde{\gamma}_{M_3}m_3(t)\\ \kappa_{\text{transl},3}m_3(t)-\tilde{\gamma}_{G_3}g_3(t)-g_3(t)\dfrac{\kappa_{\text{cat}}}{1+\kappa_S}\\ g_3(t)\dfrac{\kappa_{\text{cat}}}{1+\kappa_S}-\tilde{\gamma}_{G_3}g_3^*(t)\\ F_1(g_3^*(t),g_{80}(t))\tilde{\kappa}_{\text{transc},80}-\tilde{\gamma}_{M_{80}}m_{80}(t)\\ \kappa_{\text{transl},80}m_{80}(t)-\tilde{\gamma}_{G_{80}}g_{80}(t)\end{bmatrix},$$

$$x^S=\begin{bmatrix} \dfrac{\tilde{\kappa}_{\text{transc},3}F_1((g_3^*)^S,g_{80}^S)}{\tilde{\gamma}_{M_3}}\\ \dfrac{\tilde{\kappa}_{\text{transc},3}\kappa_{\text{transl},3}F_1((g_3^*)^S,g_{80}^S)}{\left(\dfrac{\kappa_{\text{cat}}}{1+\kappa_S}+\tilde{\gamma}_{G_3}\right)\tilde{\gamma}_{M_3}}\\ \dfrac{\tilde{\kappa}_{\text{transc},3}\kappa_{\text{transl},3}\kappa_{\text{cat}}F_1((g_3^*)^S,g_{80}^S)}{\left(\dfrac{\kappa_{\text{cat}}}{1+\kappa_S}+\tilde{\gamma}_{G_3}\right)\tilde{\gamma}_{M_3}(1+\kappa_S)}\\ \dfrac{\tilde{\kappa}_{\text{transc},80}F_1((g_3^*)^S,g_{80}^S)}{\tilde{\gamma}_{M_{80}}}\\ \dfrac{\tilde{\kappa}_{\text{transc},80}\kappa_{\text{transl},80}F_1((g_3^*)^S,g_{80}^S)}{\tilde{\gamma}_{G_{80}}\tilde{\gamma}_{M_{80}}}\end{bmatrix}\quad\text{and}$$

$$J^S=\begin{bmatrix} -\tilde{\gamma}_{M_3} & 0 & \dfrac{2(g_3^*)^S\tilde{\kappa}_{\text{transc},3}}{r\left[1+\frac{((g_3^*)^S)^2}{r}+\frac{q}{(g_{80}^S)^2}\right]^2} & 0 & -\dfrac{2q\tilde{\kappa}_{\text{transc},3}}{(g_{80}^S)^3\left[1+\frac{((g_3^*)^S)^2}{r}+\frac{q}{(g_{80}^S)^2}\right]^2}\\ \tilde{\kappa}_{\text{transl},3} & -\dfrac{\tilde{\gamma}_{G_3}+\kappa_{\text{cat}}+\tilde{\gamma}_{G_3}\kappa_S}{1+\kappa_S} & 0 & 0 & 0\\ 0 & \dfrac{\kappa_{\text{cat}}}{1+\kappa_S} & -\tilde{\gamma}_{G_3} & 0 & 0\\ 0 & 0 & \dfrac{2(g_3^*)^S\tilde{\kappa}_{\text{transc},80}}{r\left[1+\frac{((g_3^*)^S)^2}{r}+\frac{q}{(g_{80}^S)^2}\right]^2} & -\tilde{\gamma}_{M_{80}} & -\dfrac{2q\tilde{\kappa}_{\text{transc},80}}{(g_{80}^S)^3\left[1+\frac{((g_3^*)^S)^2}{r}+\frac{q}{(g_{80}^S)^2}\right]^2}\\ 0 & 0 & 0 & \tilde{\kappa}_{\text{transl},80} & -\tilde{\gamma}_{G_{80}}\end{bmatrix}.$$

The analytic expressions of the eigenvalues of the Jacobian have been calculated in `Mathematica`, and spread over a few pages. Hence an analytic investigation would be very lengthy and tedious if not impossible. Instead we choose to numerically evaluate them for combinations of parameters that place the system in the regions with either one or three steady states (as in Fig. 3). In other words, we want to check the local stability of the steady states in cases where the choice of the model parameters would lead to a single or multiple stationary points. Also, when there are three steady states we want to see how many are locally stable/unstable.

For consistency with the study from Section refbistab, the computations will use p and q as parameters. Note that the jacobian J^S is given in terms of r and q, and $r=\frac{\chi\kappa_B}{p}$. Fig. E1 illustrates a sample of our local stability study. The left panel shows the real part of the eigenvalues as $q=0.04$ and p varies between 0 and 10. The model has a single steady state with the real part of the eigenvalues always negative, *i.e.* local stability of the steady state. The plot from the right panel shows that when $q=0.001$ and $4\lesssim p\lesssim 6$ only one of the three steady states is locally unstable, and the other two are locally stable. The stability of the stationary solutions was also tested numerically (results not shown). When simulating the time evolution of the model for $3.99\leq\ p\leq 5.91$, and selecting initial conditions at random from normal distributed numbers between the mRNA and protein estimated levels in raffinose and galactose (see Table C1), the trajectory of each model variable settles to one of the two coexisting steady states.

In point of fact, more can be said about the stability of the steady states. There are two situations to consider (see Section 4.1 and Fig. E2).

- Case I: The first situation is when the first out of the three possible intersection points has a G_3-coordinate at the left of the G_3 value at which F_1^a attains its global minimum. This case is the one we encountered when exploring the model dynamics with a variety of biologically relevant parameter combinations. When changing the parameters values listed in Table C2 within one or two orders of magnitude, the G_3 value for which the global minimum of the curve F_1^a is attained was always less than 700 molecules. In glucose, which is a carbon source where we expect to have less Gal3p than in galactose, 784 Gal3p proteins have been experimentally measured (Ghaemmaghami et al., 2003). The local stability study above shows that when there is a single intersection point between the curves F_1^a and AG_3, that point is locally stable. When there are three intersection points the one in the middle is unstable, while the other two neighboring points are locally stable. However, the results of Othmer (1976), Smith (1995, Proposition 2.1, Chapter 4) can be extended to show that if there is a single steady state, *i.e.* $G_{3,1}^S$ or $G_{3,3}^S$, then it is globally stable. If there are two locally stable nodes ($G_{3,1}^S$ and $G_{3,3}^S$), then all flows are attracted to one of them.
- Case II: Theoretically, there is a second situation when a combination of model parameters is such that the first out of the three possible intersection points has a G_3-coordinate at the right of the G_3 value at which F_1^a attains its global minimum. In this framework, our model predicts a different dynamics. The first intersection point is either locally stable or a limit cycle, the middle one is unstable, and the third one is locally stable. Thus if experimental parameters could be manipulated to correspond to this case we would predict that an oscillation could be observed in the uninduced state.

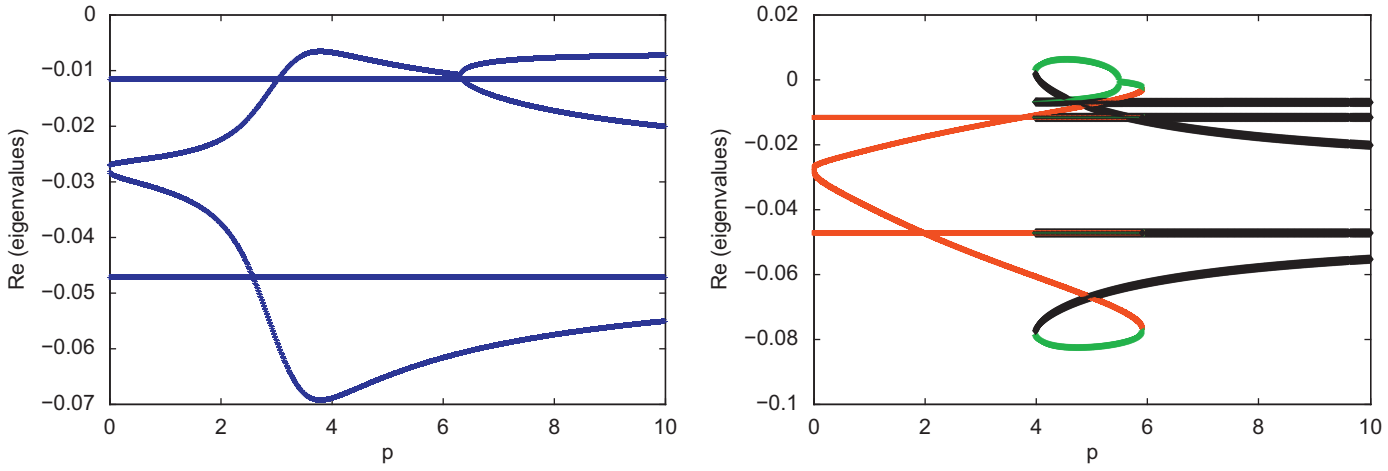

Fig. E1. Example of the local stability study for the model (D.1) stationary points. We calculate the real part of the eigenvalues of the Jacobian evaluated at the steady states when q is fixed and p is variable. Left panel corresponds to $q=0.04$. For each (p,q) pair the model (D.1) has a single steady state to which correspond five eigenvalues, all with negative real parts. When $p \lesssim 6$ two of the real parts of the eigenvalues have very close numerical values and overlap on the graph. Right panel corresponds to $q=0.001$. When $p < 3.99$ there is a single stable steady state and the system is monostable uninduced. When $3.99 \leq p \leq 5.91$ the model (D.1) has three distinct steady states, and for each of them there are five eigenvalues. For a better visualization of the number of stable versus unstable steady states, we illustrate the set of eigenvalues corresponding to a stationary point with the same color. The colors overlap when the real parts of the eigenvalues corresponding to different stationary solutions have very close numerical values. For an individual steady state only one of the three colors is above zero, *i.e.* only one of the three steady states is unstable, while the other two are stable. When $p > 5.91$ the model (D.1) is monostable induced.

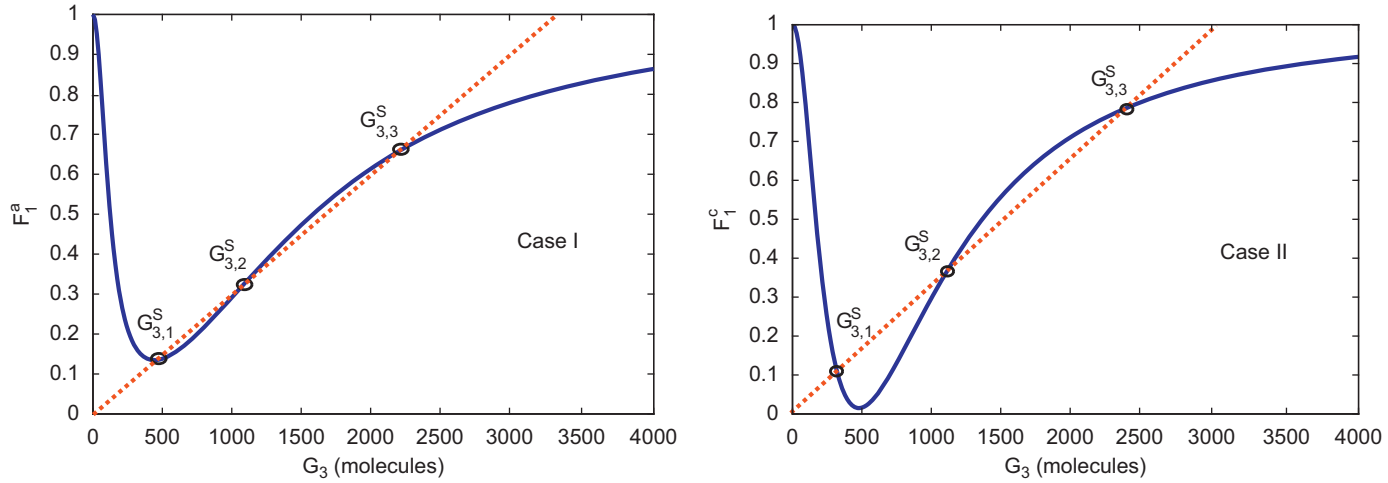

Fig. E2. Graphical illustration of the Cases I and II discussed in Section 4.1. Left panel, Case I: the following parameters have been used to plot F_1^a: $\kappa_{cat} = 300\ \text{min}^{-1}$, $K_S = 4000$ mM, $\kappa_A = 7 \times 10^{-4}$ mM, $\kappa_D = 3 \times 10^{-7}$ mM, $\kappa_{transl,3} = 12.33\ \text{min}^{-1}$, $\kappa_{transl,80} = 10.08\ \text{min}^{-1}$. Right panel, Case II: the parameters used to graph F_1^a are as in the left panel except for $\kappa_{cat} = 480\ \text{min}^{-1}$ and $\kappa_A = 5 \times 10^{-3}$ mM.

However, since our parameter estimations for the experimental situations we consider here do not seem to correspond to this case we have not considered it further here.

The mathematics behind these two cases is somewhat detailed and is beyond our purpose.

References

Acar, M., Becskei, A., van Oudenaarden, A., 2005. Enhancement of cellular memory by reducing stochastic transitions. Nature 435, 228–232.

Acar, M., Pando, B.F., Arnold, F.H., Elowitz, M.B., van Oudenaarden, A., 2010. A general mechanism for network-dosage compensation in gene circuits. Science 329, 1656–1660.

Arava, Y., Wang, Y., Storey, J.D., Liu, C.L., Brown, P.O., Herschlag, D., 2003. Genome-wide analysis of mRNA translation profiles in *Saccharomyces cerevisiae*. Proc. Natl. Acad. Sci. USA 100 (7), 3889–3894.

Belle, A., Tanay, A., Bitincka, L., Shamir, R., O'Shea, E.K., 2006. Quantification of protein half-lives in the budding yeast proteome. Proc. Natl. Acad. Sci. USA 103 (35), 13004–13009.

Bennett, M., Pang, W.L., Ostroff, N., Baumgartner, B., Nayak, S., Tsimring, L., Hasty, J., 2008. Metabolic gene regulation in a dynamically changing environment. Nature 454 (7208), 1119–1122.

Bhat, P.J., 2008. Galactose Regulon of Yeast. From Genetics to Systems Biology. Springer-Verlag, Berlin, Heidelberg.

Bhat, P.J., Hopper, J.E., 1992. Overproduction of the GALl or GAL3 protein causes galactose-independent activation of the GAL4 protein: evidence for a new model of induction for the yeast GAL/MEL regulon. Mol. Cell. Biol. 12 (6), 2701–2707.

Bhat, P.J., Murthy, T.V.S., 2001. Transcriptional control of the GAL/MEL regulon of yeast *Saccharomyces cerevisiae*: mechanism of galactose-mediated signal transduction. Mol. Microbiol. 40 (5), 1059–1066.

Bhat, P.J., Venkatesh, K.V., 2005. Stochastic variation in the concentration of a repressor activates GAL genetic switch: implications in evolution of regulatory network. FEBS Lett. 579, 597–603.

Bhaumik, S.R., Raha1, T., Aiello, D.P., Green, M.R., 2004. *In vivo* target of a transcriptional activator revealed by fluorescence resonance energy transfer. Genes Dev. 18, 333–343.

Biggar, R.B., Crabtree, G.R., 2001. Cell signaling can direct either binary or graded transcriptional responses. EMBO J. 20 (12), 3167–3176.
de Atauri, P., Orrell, D., Ramsey, S., Bolouri, H., 2004. Evolution of design principles in biochemical networks. Syst. Biol. (Stevenage) 1, 28–40.
Ghaemmaghami, S., Huh, W., Bower, K., Howson, R.W., Belle, A., Dephoure, N., O'Shea, E.K., Weissman, J.S., 2003. Global analysis of protein expression in yeast. Nature 425, 737–741.
Hawkins, K.M., Smolke, C.D., 2006. The regulatory roles of the galactose permease and kinase in the induction response of the GAL network in *Saccharomyces cerevisiae*. J. Biol. Chem. 281 (19), 13485–13492.
Holstege, F.C., Jennings, E.G., Wyrick, J.J., Lee, T.I., Hengartner, C.J., Green, M.R., Golub, T.R., Lander, E.S., Young, R.A., 1998. Dissecting the regulatory circuitry of a eukaryotic genome. Cell 95, 717–728.
Ideker, T., Thorsson, V., Ranish, J.A., Christmas, R., Buhler, J., Eng, J.K., Bumgarner, R., Goodlett, D.R., Aebersold, R., Hood, L., 2001. Integrated genomic and proteomic analyses of a systematically perturbed metabolic network. Science 292 (929), 929–934.
Jiang, F., Frey, B.R., Evans, M.L., Friel, J.C., Hopper, J.E., 2009. Gene activation by dissociation of an inhibitor from a transcriptional activation domain. Mol. Cell. Biol. 29 (20), 5604–5610.
Kulkarni, V.V., Kareenhalli, V., Malakar, P., Pao, L.Y., Safonov, M.G., Viswanathan, G.A., 2010. Stability analysis of the gal regulatory network in *Saccharomyces cerevisiae* and *Kluyveromyces lactis*. BMC Bioinf. 11, S:43.
Kumar, P.R., Yu, Y., Sternglanz, R., Johnston, S.A., Joshua-Tor, L., 2008. NADP regulates the yeast GAL induction system. Science 319, 1090–1092.
Kundu, S., Peterson, C.L., 2010. Dominant role for signal transduction in the transcriptional memory of yeast GAL genes. Mol. Cell. Biol. 30 (10), 2330–2340.
Lashkari, D.A., Derisi, J.L., McCusker, J.H., Namath, A.F., Gentile, C., Hwang, S.Y., Brown, P., Davis, R.W., 1997. Yeast microarrays for genome wide parallel genetic and gene expression analysis. Proc. Natl. Acad. Sci. USA 94, 13057–13062.
Leuther, K.K., Johnston, S.A., 1992. Nondissociation of GAL4 and GAL80 *in vivo* after galactose induction. Science 256, 1333–1335.
Lohr, D., Venkov, P., Zlatanova, J., 1995. Transcriptional regulation in the yeast GAL gene family: a complex genetic network. FASEB J. 9 (9), 777–787.
Mackey, M.C., Tyran-Kaminska, Yvinec, R., 2011. Molecular distributions in gene regulatory dynamics. J. Theor. Biol. 274, 84–96.
Melcher, K., Xu, H.E., 2001. Gal80-Gal80 interaction on adjacent Gal4p binding sites is required for complete GAL gene repression. EMBO J. 20 (4), 841–851.
Mumma, J.O., Chhay, J.S., Ross, K.L., Eaton, J.S., Newell-Litwa, K.A., Fridovich-Keil, J.L., 2008. Distinct roles of galactose-1P in galactose-mediated growth arrest of yeast deficient in galactose-1P uridylyltransferase (GALT) and UDP-galactose 4'-epimerase (GALE). Mol. Genet. Metab. 93, 160–171.
Orrell, D., Ramsey, S., Marelli, M., Smith, J., Petersen, T., de Atauri, P., Aitchison, J., Bolouri, H., 2006. Feedback control of stochastic noise in the yeast galactose utilization pathway. Physica D 217, 64–76.
Othmer, H., 1976. The qualitative dynamics of a class of biochemical control circuits. J. Math. Biol. 3, 53–78.
Parthun, M.R., Jaehning, J.A., 1992. A transcriptionally active form of GAL4 is phosphorylated and associated with GAL80. Mol. Cell. Biol. 12, 4981–4987.
Peng, G., Hopper, J.E., 2000. Evidence for Gal3p's cytoplasmic location and Gal80p's dual cytoplasmic-nuclear location implicates new mechanisms for controlling Gal4p activity in *Saccharomyces cerevisiae*. Mol. Cell. Biol. 20, 5140–5148.
Peng, G., Hopper, J.E., 2002. Gene activation by interaction of an inhibitor with a cytoplasmic signaling protein. Proc. Natl. Acad. Sci. USA 99, 8548–8553.
Platt, A., Reece, R.J., 1998. The yeast galactose genetic switch is mediated by the formation of a Gal4p/Gal80p/Gal3p complex. EMBO J. 17, 4086–4091.
Ramsey, S.A., Smith, J.J., Orrell, D., Marelli, M., Petersen, T.W., de Atauri, P., Bolouri, H., Aitchison, J.D., 2006. Dual feedback loops in the GAL regulon suppress cellular heterogeneity in yeast. Nature 38 (9), 1082–1087.
Reece, R.J., 2000. Molecular basis of nutrient-controlled gene expression in *Saccharomyces cerevisiae*. Cell. Mol. Life Sci. 57, 1161–1171.
Ruhela, A., Verma, M., Edwards, J.S., Bhat, P.J., Bhartiya, S., Venkatesh, K.V., 2004. Autoregulation of regulatory proteins is key for dynamic operation of GAL switch in *Saccharomyces cerevisiae*. FEBS Lett. 576, 119–126.
Sellick, C.A., Reece, R.J., 2005. Eukaryotic transcription factors as direct nutrient sensors. Trends Biochem. Sci. 30 (7), 405–412.
Smith, H., 1995. Monotone dynamical systems. Mathematical Surveys and Monographs, vol. 41. , American Mathematical Society, Providence, RI.
Song, C., Phenix, H., Abedi, V., Scott, M., Ingalls, B.P., Kaern, M., Perkins, T.J., 2010. Estimating the stochastic bifurcation structure of cellular networks. PLoS Comput. Biol. 6 (3), 1–11.
Timson, D.J., Ross, H.C., Reece, R.J., 2002. Gal3p and Gal1p interact with the transcriptional repressor Gal80p to form a complex of 1: 1 stoichiometry. Biochem. J. 363, 515–520.
Venkatesh, K.V., Bhat, P.J., Kumar, R.A., Doshi, P., 1999. Quantitative model for Gal4p-mediated expression of the galactose/melibiose regulon in *Saccharomyces cerevisiae*. Biotechnol. Prog. 15, 51–57.
Verma, M., Bhat, P.J., Bhartiya, S., Venkatesh, K.V., 2004. A steady-state modeling approach to validate an *in vivo* mechanism of the GAL regulatory network in *Saccharomyces cerevisiae*. Eur. J. Biochem. 271, 4064–4074.
Verma, M., Bhat, P.J., Venkatesh, K.V., 2003. Quantitative analysis of GAL genetic switch of *Saccharomyces cerevisiae* reveals that nucleocytoplasmic shuttling of Gal80p results in a highly sensitive response to galactose. J. Biol. Chem. 278 (49), 48764–48769.
Verma, M., Bhat, P.J., Venkatesh, K.V., 2005. Steady-state analysis of glucose repression reveals hierarchical expression of proteins under Mig1p control in *Saccharomyces cerevisiae*. Biochem. J. 398, 843–949.
Wightman, W., Bell, R., Reece, R.J., 2008. Localization and interaction of the proteins constituting the GAL genetic switch in *Saccharomyces cerevisiae*. Eukaryot. Cell 7 (12), 2061–2068.